

1 Nucleolar stress in *Drosophila* neuroblasts, a model for
2 human ribosomopathies

3
4

5 Sonu Shrestha Baral, Molly E. Lieux, and Patrick J. DiMario 

6
7

8 Authors' Affiliation: Department of Biological Sciences, Louisiana State University, Baton
9 Rouge, LA 70803 USA.

10

Email addresses: Sonu Shrestha Baral – sshre22@lsu.edu


11

Molly E. Lieux – mlieux@lsuhsc.edu

12

Patrick J. DiMario – pdimari@lsu.edu

13

14  To whom correspondence should be addressed (pdimari@lsu.edu)

15

16 Running title: Nucleolar stress in neuroblasts

17

18

19 Key words: Nucleolar stress, neuroblasts, *Drosophila*, Nopp140, ribosomopathy

20

21

22 **Summary Statement:**

23 Nucleolar stress (loss of ribosome production/function) in certain human stem cells or progenitor
24 cells results in disease. In fruit flies, larval Mushroom Body neuroblasts are relatively resilient to
25 nucleolar stress.

26

27

28

29

30

31

32

33

34 **ABSTRACT**

35

36 Different stem cells or progenitor cells display variable threshold requirements for functional
37 ribosomes. For instance, select embryonic neural crest cells or adult bone marrow stem cells,
38 but not others, show lethality due to failures in ribosome biogenesis or function (known as
39 nucleolar stress) in several human ribosomopathies. To determine if various *Drosophila*
40 neuroblasts display differential sensitivities to nucleolar stress, we used CRISPR-Cas9 to
41 disrupt the *Nopp140* gene that encodes two ribosome biogenesis factors (RBFs). Disruption of
42 *Nopp140* induced nucleolar stress that arrested larvae in the second instar stage. While the
43 majority of larval neuroblasts arrested development, the Mushroom Body (MB) neuroblasts
44 continued to proliferate as shown by their maintenance of deadpan, a neuroblast-specific
45 transcription factor, and by their continued EdU incorporation. MB neuroblasts in wild type
46 larvae contained more fibrillarin and Nopp140 in their nucleoli as compared to other
47 neuroblasts, indicating that MB neuroblasts stockpile RBFs as they proliferate in late
48 embryogenesis while other neuroblasts normally enter quiescence. A greater abundance of
49 Nopp140 encoded by maternal transcripts in *Nopp140*^{-/-} MB neuroblasts likely rendered these
50 cells more resilient to nucleolar stress.

51

52

53

54

55

56

57

58

59

60

61

62

63

64

65

66

67

68 INTRODUCTION

69 The nucleolus is the nuclear sub-compartment responsible for ribosomal subunit
70 biogenesis (Baßler and Hurt, 2019). Functional ribosomes in the cytoplasm of eukaryotic cells
71 consist of the small ribosomal subunit with its 18S ribosomal RNA (rRNA) assembled with 33
72 ribosomal proteins and the large ribosomal subunit with its 28S, 5.8S, and 5S rRNAs assembled
73 with 47 ribosomal proteins. This assembly is a complex choreography of reactions and
74 interactions that begins with RNA polymerase I (RNA Pol I) as it synthesizes pre-rRNA from
75 tandemly repeated ribosomal DNA (rDNA) genes. The 38S pre-rRNA in *Drosophila* undergoes
76 endonuclease cleavages to generate 18S, 5.8S+2S, and 28S rRNAs (Long and Dawid, 1980).
77 These rRNAs are chemically modified by box C/D small nucleolar ribonucleoprotein complexes
78 (snoRNPs) (2'-O-methylation) and box H/ACA snoRNPs (pseudouridylation) (Wang et al., 2002;
79 Yang et al., 2000; Bachellerie et al., 2002). Besides endonucleases and snoRNPs, subunit
80 biogenesis requires a myriad of other factors serving as RNP chaperones, RNA helicases, and
81 GTPase release factors (Kressler et al., 2010). The chaperones, often referred to as ribosome
82 biogenesis factors (RBFs), act early in ribosome assembly; they include Nopp140 (Nucleolar
83 and Cajal body phosphoprotein of 140 kDa) and treacle. While both Nopp140 and treacle are
84 found in vertebrates, only Nopp140 orthologues are expressed in all eukaryotes.

85 Ribosome biogenesis requires high energy expenditures by the cell; approximately 60%
86 of total cellular transcription is devoted to rRNA, with some 2000 ribosomes assembled per
87 minute in actively growing yeast cells (Warner 1999; Woolford and Baserga, 2013). Any
88 perturbation in ribosome biogenesis disrupts cell homeostasis; this is now called nucleolar (or
89 ribosome) stress (Golomb et al., 2014; Tsai and Pederson, 2014; Yang et al., 2018). In humans,
90 nucleolar stress due to mutations in ribosome biogenesis factors (RBFs), processing snoRNPs,
91 or the ribosomal proteins themselves results in disease states collectively called
92 ribosomopathies, of which there are several (Narla and Ebert, 2010). While each ribosomopathy
93 has its own distinct phenotypes, and several display tissue-specificity (McCann and Baserga,
94 2013), there are commonalities among them: the most prevalent dysfunctions include
95 craniofacial abnormalities, other skeletal defects, and bone marrow failures. All ribosomopathies
96 affect only certain stem cells or progenitors despite the mutation being systemic.

97 One of these ribosomopathies is the Treacher Collins Syndrome (TCS), a congenital
98 birth defect caused by haplo-insufficiency mutations in the *TCOF1* gene that encodes treacle
99 (Sakai and Trainor, 2009). A particular set of neural crest cells that normally migrate to and
100 populate pharyngeal arches I and II on day 24-25 human embryogenesis have insufficient
101 functional ribosomes in TCS individuals. This leads to p53-dependent apoptosis (Jones et al.,

102 2008). Loss of these particular neural crest cells causes the craniofacial defects. A TCS-like
103 phenotype can also result from mutations in genes encoding RNA Pol I and III subunit proteins,
104 POLR1D and POLR1C respectively (Dauwerse et al., 2011; Noack Watt et al., 2016). The
105 question is, why are only certain progenitor cells affected while others remain resilient?

106 To investigate the underlying mechanism contributing to stem cell or progenitor cell
107 specificity as seen in the human ribosomopathies, we initiated a study of nucleolar stress in
108 *Drosophila* larval neuroblasts. We wanted to determine if all neuroblast types respond similarly
109 or differentially to nucleolar stress. We typically induce nucleolar stress by depleting Nopp140.
110 Like treacle, metazoan Nopp140 orthologues contain alternating acidic and basic motifs
111 constituting a large central domain of low sequence complexity (Meier, 1996). Treacle and
112 Nopp140 also share similar roles in chaperoning C/D-box snoRNPs to the dense fibrillar
113 component of nucleoli where pre-rRNA is modified by site-specific 2'-O-methylation. Unlike
114 treacle, Nopp140 locates to Cajal bodies; thus Nopp140 may also play a role in snoRNP
115 assembly and transport to nucleoli (Gonzales et al., 2005; Hayano et al., 2003; He et al., 2015).
116 With crucial roles in ribosome biogenesis, Nopp140 depletion in *Drosophila* induces nucleolar
117 stress such that cell death occurs either by apoptosis in progenitor imaginal disc cells or by
118 autophagy in terminally differentiated polyploid gut cells (James et al., 2013, 2014).

119 The *Drosophila* larval brain comprises a diverse set of distinctive neuroblast (NB)
120 lineages generated from a fixed set of founder NBs (Homem and Knoblich, 2012; Hartenstein
121 and Wodarz, 2013). Briefly, there are four major neuroblast types in the *Drosophila* larval brain;
122 Type I NBs, Type II NBs, Mushroom Body (MB) NBs, and Optic Lobe NBs (Fig. 1A). We
123 hypothesize that upon nucleolar stress caused by the loss of Nopp140, different neuroblast
124 lineages exhibit variable phenotypes ranging from a mild loss of lineage progeny cells to
125 substantial loss of the lineage altogether. Here we show that MB neuroblasts are more resilient
126 to the effects of nucleolar stress compared to other neuroblast types. Hence, different
127 neuroblast lineages respond variably to nucleolar stress which is reminiscent of the neural crest
128 cell-specific effects caused by the loss of treacle in TCS individuals.

129

130 **MATERIALS AND METHODS**

131 **Fly stocks**

132 Fly lines used in this study included: w^{1118} (used as a wild type control, Bloomington
133 stock #3605), the third chromosome balancer stock w^* ; $Sb^1/TM3$, $P\{ActGFP\}JMR2$, Ser^1
134 (referred to as $TM3-GFP$, Bloomington stock #4534), $y^1 M\{nos-Cas9.P\}ZH-2A w^*$ (referred to as
135 $nanos-Cas9$, Bloomington stock #54591 provided by Phillip Port and Simon Bullock, MRC

136 Laboratory of Molecular Biology), w^* ; $P\{GawB\}OK107\ ey^{OK107}/In(4)\ ci^D, c^D\ pan^{ciD}\ sv^{spa-pol}$
137 (referred to as *OK107-GAL4*, Bloomington stock #854), w^* ; $P\{wor.GAL4.A\}2; Dr^1/TM3, P\{Ubx-$
138 $lacZ.w^*\}TM3, Sb^1$ (referred to as *worniu-GAL4*, Bloomington stock #56553), $w^{1118};$
139 $P\{GMR37H04-GAL4\}attP2$ (referred to as *Scabrous (Sca)-GAL4*, Bloomington stock #49969),
140 $w^{1118}; P\{y[+t7.7]\ w[+mC]=GMR38F05-GAL4\}attP2$ (referred to as *Neurotactin (Nrt)-GAL4*,
141 Bloomington stock #49383), $y^1\ w^*$; $P\{w^{+mC}=UAS-mCD8::GFP.L\}LL5, P\{UAS-mCD8::GFP.L\}2$
142 (referred to as *UAS-mCD8-GFP*, Bloomington stock #5137), *KO121 Nopp140* gene deletion line
143 (He et al., 2015), and the *UAS-TComC4.2 Nopp140* RNAi line (Cui and DiMario, 2007). Flies
144 were maintained in the laboratory at room temperature (22-24°C) on standard cornmeal-
145 molasses medium. All applicable international, national, and/or institutional guidelines for the
146 care and use of animals were followed.

147

148 **Homology Directed Insertion of *DsRed* into *Nopp140***

149 We used CRISPR-Cas9 and homology directed repair to insert the *DsRed* gene into the
150 second exon of the *Nopp140* gene. The CRISPR optimal target finder tool
151 (<http://targetfinder.flycrispr.neuro.brown.edu/>) provided 271 gRNA target sites, each 20 nt in
152 length excluding the NGG PAM sequence. Among these, six gRNAs had zero off-targets in
153 coding regions of the *Drosophila* genome. The gRNAs were additionally verified to have no off-
154 targets by the TagScan tool (Genome-wide Tag Scanner;
155 <https://ccg.epfl.ch/tagger/tagscan.html>), and the Cas-OFFinder tool (Bae et al., 2014). Two
156 gRNA targets, gRNA#52 (5'GGGCTTTGCCGGTTCCTCCGG on the minus strand of
157 *Nopp140*; with the PAM sequence underlined) and gRNA #99
158 (5'CAAGTTGGCTCCTGCTAAGAAGG on the plus strand of *Nopp140*), were chosen and used
159 for CRISPR gene editing. Successful CRISPR-Cas9 cleavage at both gRNA target sites would
160 delete 321 bps from the second exon.

161 To express these gRNAs, sense and anti-sense oligos that included *BbsI* restriction site
162 overhangs were prepared for both gRNAs by Integrated DNA Technologies (IDT; see Table 1
163 for gRNA sequences). Mixtures of sense and anti-sense oligos for each gRNA were annealed
164 (heated at 95°C for 5 min, and then cooled to room temperature over 1 hr in 1X ligation buffer).
165 The resulting double-strand DNAs were ligated separately into *pCFD3-dU6:3gRNA* at the *BbsI*
166 site. *pCFD3-dU6:3gRNA* was a gift from Simon Bullock (Addgene plasmid # 49410;
167 <http://n2t.net/addgene:49410>; RRID:Addgene_49410; (Port et al., 2014; Ren et al., 2013). The
168 resulting plasmids are referred to as *gRNA#55* and *gRNA#99* (Fig. 2A).

169 To mark the disrupted *Nopp140* gene, the *DsRed* gene was inserted at the Cas9-
170 mediated deletion site by Homology Directed Repair (HDR). We used the donor plasmid,
171 *pDsRed-attP* which was a gift from Melissa Harrison, Kate O'Connor-Giles, and Jill Wildonger
172 (University of Wisconsin-Madison) (Addgene plasmid # 51019; <http://n2t.net/addgene:51019>;
173 RRID:Addgene_51019; Gratz et al., 2014). We followed general guidelines (Gratz et al., 2014)
174 to insert the homology arms into the multiple cloning sites available on either side of the *DsRed*
175 gene in *pDsRed-attP*. The 5' and 3' homology arms from the *Nopp140* second exon were
176 prepared by PCR using forward and reverse primers listed in Table 1. These homology arms
177 flank the 321 bp deletion region described in the preceding paragraph (Fig. 2A). We first
178 inserted the 421 bp 3' arm into *pDsRed-attP* at the *Bgl*III and *Xho*I sites upstream of the *DsRed*
179 gene, and then inserted the 500 bp 5' arm at *Not*I and *Eco*RI sites downstream of the *DsRed*
180 gene. The orientation of the homology arms relative to *DsRed* should insert the *DsRed*
181 sequence by HDR such that transcription of *DsRed* is in the opposite direction relative to
182 transcription of the *Nopp140* gene (Fig. 2A). The final plasmid is referred to as *pDsRed-Donor*.
183

184 **NHEJ disruption of *DsRed* gene inserted within *Nopp140* second exon**

185 To mutate the *DsRed* gene within the *Nopp140* gene in the *J11 DsRed* fly line, we used
186 Cas9 endonuclease expressed from the *pBS-Hsp70-Cas9* plasmid, a gift from Melissa Harrison,
187 Kate O'Connor-Giles, and Jill Wildonger (Addgene plasmid # 46294;
188 <http://n2t.net/addgene:46294>; RRID:Addgene_46294; Gratz et al., 2013). To find gRNA target
189 sites within the *DsRed* gene, we again used the CRISPR optimal target finder tool which yielded
190 38 gRNA target sites that were 18-nt in length. Twelve of the 38 gRNA targets had no matches
191 to the *Drosophila* genome. Among the twelve gRNA targets, we chose gRNA#2
192 (5'GCTGAAGGTGACCAAGGGCGG on the plus strand of *DsRed*) and gRNA#3
193 (5'GCTCCCACTTGAAGCCCTCGG on the minus strand of *DsRed*). Sense and anti-sense
194 oligos for each gRNA target site were prepared by IDT (see Table 1 for sequences). Each
195 double stranded DNA encoding the respective gRNAs was separately ligated into the *pCFD3-*
196 *dU6:3gRNA* plasmid at the *Bbs*I restriction site following the same procedures described above
197 for the preparation of *gRNA#52* and *gRNA#99* plasmids. The resulting plasmids for *DsRed*
198 gene mutagenesis are *gRNA#2* and *gRNA#3*.
199

200 ***Drosophila* embryo injections**

201 All plasmids used for embryo injections were extracted from transformed *E. coli* cells
202 using a plasmid Midiprep kit from ThermoFisher Scientific. To disrupt the *Nopp140* gene, the

203 plasmid injection mixture contained 15 ng/ μ L of *gRNA#52*, 15 ng/ μ L of *gRNA#99*, and 230
204 ng/ μ L of *pDsRed-Donor*. The mixture was injected into homozygous *nanos-Cas9* transgenic
205 embryos. To disrupt the *DsRed* gene, the CRISPR injection mixture contained 75 ng/ μ L of
206 *gRNA#2*, 75 ng/ μ L of *gRNA#3*, and 350 ng/ μ L of *pBS-Hsp70-Cas9*. This mixture was injected
207 into *J11 DsRed/TM3-GFP* embryos. All injections were performed by GenetiVision Corporation
208 (Houston, TX).

209

210 **PCR verification of Homology Directed Cas9-mediated donor sequence insertion**

211 Approximately 30 healthy well-fed adults were homogenized in 100 mM Tris-HCl (pH
212 7.5), 100 mM EDTA, 100 mM NaCl, and 0.5% SDS, followed by 30 min incubation at 70°C.
213 Genomic DNA was precipitated in a 1:2 ratio of 5 M KOAc : 6 M LiCl on ice for 10 min, followed
214 by phenol-chloroform purification and ethanol precipitation. PCR reactions contained 20-70 ng
215 of genomic DNA, 0.40 μ M of each primer, 0.20 mM of each dNTP, 0.50 mM of MgCl₂, 1 X
216 Phusion GC Buffer, and 0.40 unit of Phusion high-fidelity DNA polymerase (M0530S, New
217 England BioLabs). Amplification was performed in a BIO-RAD C1000 Thermal Cycler (cycling
218 conditions: 32 cycles of denaturation for 30 sec at 95°C, annealing for 30 sec at 62°C, and
219 elongation at 72°C for 1 min 20 sec). Primers used for PCR verification were *DsRed-Reverse*
220 and *Nopp140-Exon2-1556*. Their sequences are provided in Table 1.

221

222 **Sequence analyses**

223 PCR products were extracted from agarose gels using phenol-chloroform, ethanol
224 precipitated, and then sequenced using a BigDye Terminator Cycle Sequencing kit v.3.1 and an
225 ABI 3130XL Genetic Analyzer (Applied Biosystems). Sequencing primers are indicated
226 wherever the sequence reads are provided. Sequences were analyzed and aligned using CLC
227 Sequence Viewer (QIAGEN Bioinformatics).

228

229 **RT-PCR analysis**

230 Larvae at day 1-2 after larval hatching (ALH) or day 5-7 ALH were collected from well-
231 yeasted grape juice plates, placed into an Eppendorf tube, and rinsed with distilled water to
232 remove yeast and other debris. Total RNA was extracted from wild-type or *Nopp140*^{-/-} larvae
233 using TRIzol (Invitrogen) according to the manufacturer's recommendations. First-strand cDNA
234 synthesis was performed using M-MuLV Reverse Transcriptase (NEB M0253S) according to
235 manufacturer's recommendations with either oligo(dT) primers or gene-specific reverse primers

236 (same as the reverse primers used in PCR). Oligo(dT) primers were used to synthesize the first-
237 strand cDNA of *Hsp26*, *RpL32*, and *Actin5C*. Gene-specific reverse primers were used for the
238 *ETS* and *ITS2* regions of pre-ribosomal RNA. Specific forward and reverse PCR primers are
239 described in Table 1.

240

241 **Immunostaining and fluorescence microscopy**

242 Larval brains and other tissues were dissected directly into fixation Buffer B, pH 7.0-7.2
243 (16.7 mM $\text{KH}_2\text{PO}_4/\text{K}_2\text{HPO}_4$, 75 mM KCl, 25 mM NaCl, 3.3 mM MgCl_2) (de Cuevas and
244 Spradling, 1998) with 2% paraformaldehyde (from a freshly prepared 10% stock). Tissues were
245 fixed for 30-35 min total starting from the point when the dissection commenced. All washings
246 were done with PBS with 0.1% TX-100 detergent. The blocking solution was 3% BSA prepared
247 in PBS with 0.1% TX-100 which was also used for preparing dilutions of primary and secondary
248 antibodies. In all cases, tissues were incubated in the primary antibody overnight at 4°C on a
249 shaker, and in the secondary antibody for 4 hr at 4°C on a shaker. Primary antibodies included
250 the polyclonal guinea pig anti-Nopp140-RGG (Cui and DiMario, 2007) used at 1:100, a rat
251 monoclonal anti-Deadpan (abcam, 195173, stock 1 mg/ml) used at 1:250, the mouse
252 monoclonal anti-fibrillarin mAb 72B9 (Reimer et al., 1987; hybridoma supernatant used without
253 dilution), the mouse monoclonal anti-prospero (deposited at the DSHB by C.Q. Doe; DSHB
254 Hybridoma Product: Prospero MR1A) used at 1:50, and the mouse monoclonal anti-discs large
255 (dlg) (deposited at the DSHB by C. Goodman; DSHB Hybridoma Product: 4F3 anti-discs large)
256 used at 1:30. Secondary antibodies included the Alexa Fluor 546 conjugated goat anti-rat (A-
257 11081, ThermoFisher Scientific) used at 1:1000, the Alexa Fluor 594 conjugated goat anti-
258 guinea pig (A-11073, ThermoFisher Scientific) used at 1:500, and the Dylight 488 conjugated
259 goat anti-mouse (35503, ThermoFisher Scientific) used at 1:500. Tissues were counter-stained
260 with 4',6-diamino-2-phenylindole (DAPI, Polysciences) at 1 $\mu\text{g}/\text{mL}$. To image the tissues, we
261 used either a conventional fluorescence microscope, a Zeiss Axioskop equipped with a SPOT
262 RTSE digital camera, or a Leica SP8 Confocal Microscope equipped with the White Light Laser
263 system in the Shared Instrumentation Facility (SIF) at Louisiana State University.

264

265 **EdU labeling**

266 For 5-ethynyl-2-deoxyuridine (EdU) labeling, larval brains were dissected in PBS
267 (without any detergent or azide), and within 5 min of dissection, the brains were incubated with
268 20 μM EdU in PBS for 30 min or 2 hr at room temperature. The tissues were then fixed in Buffer
269 B with 2% paraformaldehyde (described above) for 30 min at room temperature. EdU

270 incorporated into S-phase cells was detected by a Click-iT Alexa Fluor 488 EdU imaging kit
271 (Invitrogen) according to the manufacturer's recommendation. EdU was also detected by Alexa
272 Fluor 594-Azide (Product No.1295, AF 594 Azide from Click Chemistry Tools) used with the
273 reagents provided by Invitrogen Click-iT EdU imaging kit. Following EdU labeling, the larval
274 brains were immunostained with antibodies followed by DAPI counterstaining.

275

276 **Determination of nuclear area**

277 The 2D confocal images of the *Nopp140*^{-/-} and wild-type larval brains at day 2-3 ALH
278 were analyzed using Fiji software. After setting scale for each image, the free hand selection
279 tool was used to draw outlines of each nucleus, and the nuclear area was subsequently
280 recorded. Deadpan-stained larval brains were used to determine the nuclear area of
281 neuroblasts. Neuronal nuclear area was obtained from the DAPI-stained larval brains. The
282 nuclear areas were plotted into a box-scatter plot using Microsoft Excel, and a Student's t-test
283 (one-tailed) was performed on the data.

284

285 **RESULTS**

286 **CRISPR for homology directed repair (HDR) to disrupt the *Nopp140* gene**

287 We used CRISPR-Cas9 to delete a target sequence of 321 bps from the second exon of
288 the *Nopp140* gene. A cocktail of two *gRNA* plasmids and the *DsRed-Donor* plasmid was
289 injected into embryos homozygous for the *nanos::Cas9* transgene (Fig. 2A). The *gRNAs*
290 directed the Cas9-mediated deletion, and HDR inserted the *DsRed* gene across the deletion
291 (Fig. 2A). *DsRed* then served as a selectable marker for the disrupted *Nopp140* gene; it was
292 expressed from the *3xP3* eye promoter which is normally active in the entire embryonic and
293 larval brain, Bolwig's organ, hind gut, anal pads, and adult eyes. We recovered seven
294 independent *Nopp140* disruption lines (*J11*, *J47*, *J54*, *J60*, *K13*, *M6*, *M20*) using the red
295 fluorescence eye phenotype. Each of the seven *Nopp140* disrupted chromosomes was
296 maintained over the *TM3-GFP* balancer chromosome which carries a wild type copy of
297 *Nopp140*. The *DsRed* insertion was verified by genomic PCRs (Fig. 2B). The expected 1836 bp
298 PCR product was amplified in all seven *Nopp140* insertion alleles, with *w¹¹¹⁸* acting as a wild
299 type negative control (Fig. 2A,B). Among the seven lines initially recovered, *J11^{DsRed}/TM3-GFP*
300 was backcrossed with the *Sb¹/TM3-GFP* fly line for at least six generations to eliminate possible
301 off-target mutations in the *J11^{DsRed}* line.

302 The *GFP* reporter gene on the *TM3* balancer chromosome is expressed in a small
303 cluster of larval midgut cells that are easily identifiable. Therefore, with *inter se* crosses of

304 *J11^{DsRed}/TM3-GFP* stock flies, we hand-selected larvae that were homozygous for *J11^{DsRed}*, but
305 selected against sibling larvae heterozygous for *J11^{DsRed}/TM3-GFP* with prominent GFP signals
306 in their midgut.

307 To conduct multi-channel immunofluorescence of the *Drosophila* brain, we again used
308 CRISPR-Cas9 but now with Non-Homologous End Joining (NHEJ) to disrupt the *DsRed* gene
309 inserted in the *J11^{DsRed}* allele. A cocktail of two gRNA plasmids and the *pBS-Hsp70-Cas9* vector
310 injected into *J11^{DsRed}/TM3* embryos produced several independent fly lines with mutations in
311 *DsRed* (Supplementary Fig. S1). We sequenced the second exon region in two of these lines,
312 *A5* and *A7*, and verified that each had a short deletion at the gRNA#3 target site within the
313 *DsRed* gene (Supplementary Fig. S1). The *A7-J11^{non-DsRed}* fly line was again back-crossed six
314 times to deplete any possible off-site targets. Either the original *J11^{DsRed}* fly line or its derived
315 *A7-J11^{non-DsRed}* line was used for the experiments described below.

316 We next performed RT-PCR analyses to test if the disrupted *Nopp140* gene was
317 transcribed in homozygous *A7-J11^{non-DsRed}* larvae (day 1-2 ALH) (Fig. 2C). The reverse primer
318 referred to as *pDsRed* in Fig. 2C annealed to the *pDsRed-attP* plasmid sequence a few base
319 pairs downstream of the junction between the *Nopp140* second exon and the *DsRed* donor
320 sequence. No transcripts containing *DsRed-att* sequences were detected in the total RNA
321 samples prepared from homozygous *A7-J11^{non-DsRed}* larvae 1-2 day, similar to the *w¹¹¹⁸* sample
322 that served as a negative control (Fig. 2C, but see below for a positive control). Nonsense-
323 mediated decay (NMD) would likely degrade *Nopp140* pre-mRNAs transcribed from the
324 disrupted gene as they would likely contain premature stop codons within the *pDsRed-att*
325 sequences, or these pre-mRNAs may be improperly/incompletely spliced (Garneau et al.,
326 2007). This lack of RT-PCR products eliminates the likelihood of a dominant-negative effect due
327 to the production of truncated *Nopp140* proteins encoded by the disrupted *Nopp140* gene. In
328 summary, hand-selected larvae homozygous for the *Nopp140 J11^{non-DsRed}* allele provide a null
329 genotype (*Nopp140*/-) systemic throughout the larvae.

330 We next determined if there were maternal wild type *Nopp140* transcripts present in the
331 RNA preparations isolated from the same homozygous *A7-J11^{non-DsRed}* 1-2 day ALH larvae used
332 for the RT-PCRs described in the preceding section. We performed these second RT reactions
333 using a reverse primer (*Exon2*, blue in Fig. 2C) that anneals to the *Nopp140* second exon a few
334 base pairs upstream of the junction between the *Nopp140* second exon and the *DsRed* donor
335 sequence. Since *Nopp140* transcripts harboring *DsRed* sequences were undetectable in these
336 larvae, first strand cDNAs primed with *Exon2* should indicate the presence of maternal *Nopp140*
337 transcripts in homozygous *J11^{DsRed}* larvae, and thus serve as a positive control for the initial RT-

338 PCRs that showed an absence of *DsRed-att*-containing transcripts. These second RT-PCRs
339 showed that maternal *Nopp140* transcripts were indeed present in the *Nopp140*^{-/-} larvae at day
340 1-2 ALH. The abundance of maternal *Nopp140* transcripts in the *Nopp140*^{-/-} larvae was about
341 half that seen in wild type larvae, suggesting that both maternal and zygotic *Nopp140* transcript
342 pools exist in early wild type larvae (Fig. 2C).

343 As additional controls (Fig. 2D), RT-PCR analyses of the External Transcribed Spacer
344 (*ETS*) and the Internal Transcribed Spacer 2 (*ITS2*) sequences within pre-rRNA showed that
345 their levels were unaffected in homozygous *J11*^{*DsRed*} larvae at day 1-2 ALH and at day 5-7 ALH.
346 This indicates that loss of Nopp140 had no effect on rDNA transcription, which agreed with our
347 earlier observations with a *pBac*-generated *Nopp140*^{KO121} deletion line (He et al., 2015).
348 Furthermore, *Hsp26* transcript levels were upregulated in homozygous *J11*^{*DsRed*} larvae at both
349 day 1-2 and day 5-7 ALH, whereas the wild-type larvae had almost undetectable levels of
350 *Hsp26* transcript (Fig. 2D). Overexpression of *Hsp26* in homozygous *J11*^{*DsRed*} larvae as early as
351 day 1 ALH indicated a cellular stress response due to the effects of Nopp140 loss (e.g., Wang
352 et al., 2004). As final controls, we accessed *RpL32* and *Actin5C* transcript levels: while *RpL32*
353 transcript levels remained unchanged between the wild-type and homozygous *J11*^{*DsRed*} samples
354 and between biological replicates, *Actin5C* transcript levels fluctuated slightly within the samples
355 and between biological replicates for reasons that remain uncertain.

356

357 **Maternal Nopp140 protein is reduced in early *J11 Nopp140*^{-/-} larval brains**

358 Since the RT-PCR analyses showed that maternal *Nopp140* transcripts persisted in the
359 homozygous *J11*^{*DsRed*} larvae at day 1-2 ALH, we wanted to test if the Nopp140 protein could be
360 detected in their brain and gut tissues as well. To do this, we immunostained homozygous *A7*-
361 *J11*^{*non-DsRed*} larvae and wild-type larvae with an antibody directed against Nopp140-RGG, one of
362 the two Nopp140 isoforms in *Drosophila*. This antibody was raised against a synthetic peptide,
363 the sequence of which is unique to the carboxyl tail region of Nopp140-RGG (see Cui and
364 DiMario, 2007). An antibody directed against the carboxyl terminus of the other isoform,
365 Nopp140-True, has proven much weaker, and was not used here. At day 1-2 ALH, the anti-
366 Nopp140-RGG antibody labeled nucleoli in homozygous *J11*^{*non-DsRed*} larval brain and midgut, but
367 at lower levels compared to the same wild type tissues (Fig. 3, panels a-d for brain, e-h for gut
368 tissue). The homozygous *A7-J11*^{*non-DsRed*} larval brains had fewer and smaller-sized nucleoli
369 compared to nucleoli in wild-type brains at day 1-2 ALH (Fig. 3, compare panels a and c). Four
370 large-sized nucleoli per brain lobe were routinely detected in the anterior of wild-type larval
371 brains, and we speculated these were the Mushroom Body (MB) neuroblasts that do not

372 undergo quiescence, but continue to divide throughout the embryo-to-larva transition (arrow in
373 Fig. 3a). However, we did not observe this preferential labeling in homozygous *A7-J11^{non-DsRed}*
374 brains. By day 4-5 ALH, nucleolar labeling by anti-Nopp140-RGG was noticeably reduced in
375 homozygous *A7-J11^{non-DsRed}* larval brains and gut tissues as compared to the wild type tissues
376 (Fig. 3, panels i-l for brain, m-p for midgut). These results indicated that at least the Nopp140-
377 RGG isoform encoded presumably by maternal transcripts persisted in the first two days of
378 homozygous *A7-J11^{non-DsRed}* larval development, but then diminished in most cells as these
379 larvae aged.

380

381 **Embryonic and larval survivability with complete or partial elimination of Nopp140**

382 The *Nopp140* disruption lines were maintained using the third chromosome balancer,
383 *TM3*, which carries a wild type *Nopp140* gene. Embryos homozygous for *TM3* are non-viable,
384 hence *inter se* crosses within the *J11^{DsRed}/TM3* fly stock should produce 50%
385 *Nopp140^{DsRed}/TM3* larvae and 25% homozygous *J11^{DsRed}* larvae (the number of hatched larvae
386 ÷ total number of eggs collected). However, if the disrupted *Nopp140* gene causes embryonic
387 lethality, we would expect frequencies less than 50% and 25%, respectively. We found that only
388 20.8% of total eggs developed into larvae that were *J11^{DsRed}/TM3* versus the expected 50%
389 (Fig. 4A), and only 7.1% of the total eggs developed into larvae that were homozygous for
390 *J11^{DsRed}* versus the expected 25% (Fig. 4A). These data indicated that loss of Nopp140 leads to
391 partial embryonic lethality not only for the *homozygous J11^{DsRed}* genotype, but more interestingly
392 for the heterozygous *J11^{DsRed}/TM3* genotype. The observation indicated for the first time that the
393 *Nopp140*^{-/+} genotype exhibits haplo-insufficiency in *Drosophila*, similar to the *Tcof1*^{-/+} genotype
394 in the human Treacher Collins Syndrome.

395 We earlier described growth arrest and lethality in second instar larvae that were
396 homozygous for our original *pBac*-mediated *Nopp140^{KO121}* deletion (He et al., 2015). Because of
397 the particular *pBac* elements available at the time, we had to delete the 3' end of the
398 downstream gene, *P5CDh1* (He and DiMario, 2011), and this constantly forced us to control for
399 the carboxyl truncation in the protein product when assessing the loss of Nopp140. Here, we
400 assessed survivability of larvae homozygous for *J11^{DsRed}*. Similar to our earlier findings (He et
401 al. 2015), we found that ~50% of the homozygous *J11^{DsRed}* larvae died by day 6 (which is when
402 the pupal stage normally begins) (Fig. 4B). The remaining 50% remained as second instar
403 larvae; they failed to grow or molt. The number of surviving homozygous *J11^{DsRed}* larvae
404 dwindled over time, but interestingly, some lingered up to day 24 (Fig. 4B).

405 We also depleted Nopp140 using the UAS-GAL4 system to express siRNAs. In the past
406 we showed that *daughterless::GAL4>UAS::TComC4.2* depleted ~70% of the *Nopp140*
407 transcripts (Cui and DiMario, 2007). Using the neuroblast-specific *worniu::GAL4* driver (*worniu-*
408 *GAL4>UAS::TComC4.2*), we found embryonic survivability was ~46%, while the wild type
409 embryo survival rate was ~86% (Fig. 4C). Interestingly, the surviving
410 *worniu::GAL4>UAS::TComC4.2* larvae developed into viable and fertile adults. While the *worniu*
411 promoter is active in all embryonic and larval neuroblasts, its peak expression is in 6-12 hr
412 embryos, perhaps explaining the survivability of nearly half the *worniu::GAL4>UAS::TComC4*
413 embryos beyond this embryonic stage.

414

415 **Brain hypoplasia upon nucleolar stress**

416 We found that larval brain development was severely impaired upon loss of Nopp140
417 either by gene disruption (i.e., homozygous *J11^{DsRed}*) or by neuron-specific RNAi depletion.
418 During the early larval stage (day 1-2 ALH), homozygous *J11^{DsRed}* brains were morphologically
419 comparable in size to brains from newly hatched wild-type larvae. The mutant's brain continued
420 to grow from day 3-6 ALH, but more slowly compared to wild-type larval brains (Fig. 5A).
421 Beyond day 5-6 ALH, homozygous *J11^{DsRed}* larval brains failed to grow. This was similar to what
422 we saw in our original *Nopp140^{KO121}* deletion (He et al., 2015) (Fig. 5A). Likewise, brain growth
423 was impaired in larvae upon RNAi-mediated depletion of Nopp140 using a pan-neuronal *GAL4*
424 driver (*Neurotactin::GAL4>UAS::TComC4.2*) (Fig. 5B).

425 To see where growth was interrupted, we immunostained brains from homozygous
426 *J11^{DsRed}* larvae and wild type larvae at day 2-3 ALH with an antibody against *discs large* (anti-
427Dlg). This antibody stains axon bundles (the neuropil), but not the cell body mass which we
428 counter-stained with DAPI. Neuropils within the two central brain lobes were reduced in
429 homozygous *J11^{DsRed}* brains as compared to wild type brains, but there were no observable
430 physical defects in the ventral nerve cord (VNC) neuropil of homozygous *J11^{DsRed}* larvae when
431 compared to wild type larvae. Besides the reduced central brain lobe neuropils, we found the
432 cell body mass of the central brain lobe was also reduced in homozygous *J11^{DsRed}* brains when
433 compared to wild type brains (Fig. 5C).

434

435 **Reduced neuroblast numbers and proliferation upon nucleolar stress**

436 We hypothesized that the hypoplasia in *Nopp140^{-/-}* larval brains was due to either a
437 reduction in NB numbers, a reduction in their proliferative capacity, or both. To assess these
438 possibilities, we first performed a Click-iT EdU labeling assay on living brains. EdU is a

439 thymidine analog which is incorporated into genomic DNA during S-phase of the cell cycle, and
440 hence these cells are committed to cell division. The assay used a 2 hr EdU pulse in wild type
441 and homozygous *A7-J11^{non-DsRed}* larval brains at 1, 2-3, and 6 days ALH. After pulse-labeling,
442 brains were fixed with paraformaldehyde, and the EdU residues were fluorescently labeled by
443 Click-iT chemistry. We then immunostained the same brains with anti-Deadpan to visualize the
444 number and distribution of neuroblasts. Deadpan (Dpn) is a neuroblast-specific transcription
445 factor necessary for self-renewal properties.

446 Anti-Dpn labeling showed that NBs were present in homozygous *J11^{non-DsRed}* larval brains
447 from all age groups, however their numbers were consistently reduced compared to the wild-
448 type brains of the same age (Fig. 6; compare homozygous *J11^{non-DsRed}* panels a, g, and m with
449 wild-type panels d, j, and p). This suggested that fewer neuroblasts in the homozygous *J11^{non-}*
450 *DsRed* larval brains likely contributed to the observed hypoplasia. Strikingly, in homozygous
451 *J11^{non-DsRed}* larvae at day 1 and day 2-3 ALH, we consistently noticed four NBs in each central
452 brain lobe that showed prominent anti-Dpn labeling compared to the surrounding Dpn-stained
453 NBs (Fig. 6; arrows in panels a and g). These four NBs were visible in the wild-type brains as
454 well, but only in brains from day 1 ALH larvae (Fig. 6; arrows in panel d).

455 EdU labeling displayed NBs and their progeny GMCs that were in S-phase. Overall,
456 homozygous *J11^{non-DsRed}* larval brains had fewer EdU-positive cells as compared to the wild-type
457 brains in all three examined age groups (Fig. 6; compare homozygous *J11^{non-DsRed}* panels b, h,
458 and n with wild-type panels e, k, and q). The same subset of the EdU-positive cells in both
459 homozygous *J11^{non-DsRed}* and wild-type brains were identified as NBs by the anti-Dpn nuclear
460 staining. Other than the four NBs that co-labeled with EdU and anti-Dpn in both homozygous
461 *J11^{non-DsRed}* and wild-type larval brains at day 1 ALH, there were also fewer EdU-positive GMCs
462 in the homozygous *J11^{non-DsRed}* brains compared to the wild-type brains (Fig. 6; compare
463 *Nopp140^{-/-}* panels a, b with wild type panels d, e). This suggested a slower rate of NB
464 proliferation in the homozygous *J11^{non-DsRed}* larval brains compared to the wild-type NBs.

465 At day 2-3 ALH, we consistently observed only the four anterior NBs that co-labeled
466 with both EdU and anti-Dpn in homozygous *J11^{non-DsRed}* brains (Fig. 6, arrows in panels g and h).
467 We predicted that these NBs were the MB NBs based on their location and consistency in
468 number. Wild-type larval brains, however, had more EdU-positive and Dpn-positive cells,
469 suggesting that the majority of NBs had exited quiescence and started to proliferate as expected
470 (Fig. 6, panels j and k). At day 1 ALH, we also noticed other EdU-positive cells in the lateral
471 regions of the central brain lobes from both homozygous *J11^{non-DsRed}* and wild-type larvae (Fig.
472 6, arrowheads in panels b and e). These should be the Antennal Lobe (AL) NBs. They were

473 occasionally detected in central brain lobes of day 2-3 ALH homozygous *J11^{non-DsRed}* (Fig. 6,
474 arrowheads in panel h).

475 These observations indicate that upon nucleolar stress, only a subset of neuroblasts and
476 GMCs proliferate in homozygous *J11^{non-DsRed}* brains although at a slower rate, and give rise to
477 lineages that are comparatively smaller than those in wild type brains under non-stressed
478 conditions. Indeed, using an antibody against Prospero, a nuclear marker specific for GMCs and
479 their descendent glia and neurons, we found significantly fewer GMC populations in the
480 homozygous *J11^{non-DsRed}* brains than in wild-type brains at day 1-2 and 6-7 ALH (Supplementary
481 Fig. S2). Additionally, we found that the nuclear volumes in the NBs and neurons were
482 noticeably reduced in homozygous *J11^{non-DsRed}* larval brains compared to wild-type larval brains
483 at day 2-3 ALH (Supplemental Fig. S3). Thus, upon nucleolar stress, larval brain hypoplasia
484 resulted from the loss of mostly Type I and II neuroblasts, the reduced size of remaining
485 neuroblasts and neurons, and the inability of these neuroblasts to proliferate.

486

487 **Mushroom body neuroblasts are resilient to nucleolar stress**

488 To test if the four anterior EdU-positive NBs were in fact MB NBs, we used a MB
489 lineage-specific *GAL4* driver to express a GFP-tagged plasma membrane reporter protein,
490 mCD8-GFP (*OK107::GAL4>mCD8::GFP*), and again performed a 30 min co-EdU-labeling in
491 brains from both homozygous *J11^{non-DsRed}* and control larvae at day 3 ALH (see the genetic
492 cross scheme in Supplemental Fig. S4). EdU labeling showed many S-phase cells in the wild
493 type larval brains; a subset of these cells located within the mCD8-GFP-positive MB-lineage cell
494 cluster (Fig. 7; panel c). In the homozygous *J11^{non-DsRed}* larval brains at day 3 ALH, EdU-positive
495 cells in the anterior region of the CBs were always located within the MB lineage-cell cluster as
496 identified by mCD8-GFP (Fig. 7; panel g). This suggested that the four Dpn-positive and EdU-
497 positive NBs that we observed in homozygous *J11^{non-DsRed}* larval brains at day 2-3 ALH (Fig. 6;
498 panel g and h) were indeed MB NBs. The combined results of Figs. 6 and 7 suggest that the MB
499 NBs are more resilient to nucleolar stress induced by the loss of Nopp140 as compared to other
500 NBs within these brains.

501

502 **Mushroom body neuroblasts in the *Nopp140*^{-/-} larval brain retain nucleolar fibrillarin**

503 Nopp140 is a chaperone for C/D-box snoRNPs that catalyze 2'-O-methylation of pre-
504 rRNA during ribosome biogenesis. Previous work in our lab showed that the C/D-box snoRNP
505 methyl-transferase, fibrillarin, redistributes to the nucleoplasm upon complete loss of Nopp140
506 in larval tissues homozygous for the *Nopp140*^{KO121} gene deletion. Loss of fibrillarin from the

507 nucleoli caused a reduction in 2'-O-methylation of pre-rRNA clearly indicating nucleolar
508 dysfunction, even though gross nucleolar morphology and rDNA transcription remained normal
509 (He et al., 2015). Since MB NBs, but not others, continue to divide in *Nopp140*^{-/-} larval brains at
510 day 2-3 ALH, we predicted that MB NBs might retain fibrillarin within their nucleoli, while other
511 NBs and their lineages redistribute fibrillarin to the nucleoplasm. To test this, we immunostained
512 brains from homozygous *J11^{non-DsRed}; OK107::GAL4>mCD8::GFP* larvae and wild-type
513 *OK107::GAL4>mCD8::GFP* larvae (see the genetic cross scheme in Supplemental Fig. S4) with
514 anti-fibrillarin at day 3 ALH. While anti-fibrillarin stained nucleoli with minimal nucleoplasmic
515 labeling in the wild-type larval brains (Fig. 8), it labeled the nucleoplasm in the majority of brain
516 cells in homozygous *J11^{non-DsRed}* larval brains, except for a small number of cells located within
517 the MB-lineage as marked by mCD8-GFP labeling; these cells showed clear nucleolar labeling
518 with anti-fibrillarin, even though there was some nucleoplasmic labeling (Fig. 8). This result
519 indicates that the MB-lineage cells, and not others, are able to retain at least some nucleolar
520 fibrillarin, indicating that their nucleoli are partially functional.

521

522 **A transcriptomics perspective**

523 With MB NBs apparently retaining fibrillarin, we asked how much Nopp140 and fibrillarin
524 are normally present within wild type MB neuroblasts relative to other neuroblasts. As an initial
525 query, we analyzed the NB-lineage specific transcriptome data set from Yang et al. (2016) who
526 performed a cell-type specific RNA-seq analysis for *Drosophila* larval neuroblasts (non-selective
527 “all” NBs, MB NBs, AL NBs, and Type II NBs), neurons, and glia. We found the expression
528 levels of four RBFs (*Nopp140*, *fibrillarin*, *Nop56*, and *Nop60B*) were higher in the MB NBs
529 compared to the AL NBs and Type II NBs (Fig. 9A). We also checked the expression levels of
530 the four *Drosophila* Nucleostemin orthologues (NS1 – NS4) (Kaplan et al., 2008; Rosby et al.,
531 2009; Hartl et al., 2013; Wang and DiMario, 2017). Mammalian nucleostemin (NS) is a nucleolar
532 GTP-binding protein originally described in embryonic and neuronal stem cells and in certain
533 cancer cells that can regulate both ribosome production and cell cycle progression (Tsai, 2011).
534 We found *NS1*, *NS2*, and *NS4*, but not *NS3* expressed at higher levels in the neuroblasts than
535 in neurons (Fig. 9B). As controls, we checked the expression levels of *Deadpan* which encodes
536 a NB-specific transcription factor, *Prospero* which encodes a NB- and GMC-specific
537 transcription factor, and *Elav* which encodes a *Drosophila* neuron-specific protein. As expected,
538 *Deadpan* and *Prospero* expression levels were higher in NBs compared to neurons, and *Elav*
539 expression was higher in neurons compared to NBs (Fig. 9C).

540 To inquire if differences exist in the expression levels for genes encoding ribosomal

541 proteins in different NB lineages, we again analyzed the transcriptomic data set of Yang et al.
542 (2016). Out of 92 genes encoding ribosomal proteins (recall that ~80 different proteins
543 constitute an intact ribosome), 47 genes were preferentially expressed in MB NBs compared to
544 AL NBs, Type II NBs, and neurons (Supplemental Fig. S5). Noticeably, *RpL41* had the highest
545 expression levels among all ribosomal protein genes in all brain cell types examined, but *RpL41*
546 transcripts levels were significantly higher in the MB NBs (indicated by an asterisk in
547 Supplemental Fig. S5). Enhanced expression of *RpL41* and the other 46 genes in MB NBs
548 suggests that their ribosomes may be different from those in other NB lineages.

549

550 **DISCUSSION**

551 A wealth of knowledge exists for *Drosophila* neurogenesis making it possible to analyze
552 developing brains at the level of individual neuroblast lineages (Birkholz et al., 2015; Egger et
553 al., 2008; Hartenstein and Wodarz, 2013; Homem and Knoblich, 2012; Urbach and Technau,
554 2003). We asked if Type I and II neuroblasts, Mushroom Body (MB) neuroblasts, Optic Lobe
555 neuroblasts, and Antennal Lobe (AL) neuroblasts are affected variably upon nucleolar stress, as
556 are stem cells and precursor cells in the human ribosomopathies. To induce nucleolar stress,
557 we used CRISPR-Cas9 to disrupt the *Nopp140* gene which encodes two isoforms that function
558 as early RBFs. *Drosophila* larvae homozygous for the *Nopp140* disruption allele, *J11^{non-DsRed}*,
559 showed smaller brains by day 4 ALH (Fig. 5A). These *Nopp140*^{-/-} larvae arrested in the second
560 instar stage, and while some lingered to day 24 ALH; none of them survived (Fig. 4B).

561 Compared to wild-type brains, *Nopp140*^{-/-} larval brains at day 2-3 ALH had far fewer
562 proliferating NBs. However, deadpan antibody labeling and EdU labeling of homozygous *J11^{non-}*
563 *DsRed* larvae showed that MB neuroblasts, and in some cases the AL neuroblasts, proliferated
564 through the embryo-to-larva transition and continued to proliferate at day 2-3 ALH as other
565 neuroblast lineages remained arrested (Fig. 6). Hence, MB NBs exhibited resilience to nucleolar
566 stress due to loss of zygotic *Nopp140* gene expression.

567

568 **Ontogenesis of the Mushroom Body Neuroblast Lineages**

569 Insect MBs are central hubs for olfactory sensory input, learning, and memory (Thum
570 and Gerber, 2019). Formation of the MBs begins during embryogenesis during which each MB
571 NB differentially expresses unique combinations of the regulatory genes (Kunz et al., 2012;
572 Yang et al., 2016). As far as we know, none of these gene products have direct links to
573 ribosome production. During the embryo-to-larva transition, only the four MB NBs and one
574 Antennal lobe (AL) NBs continue to proliferate independently of dietary nutrients and PI3-kinase

575 activity (Kunz et al., 2012; Prokop and Technau, 1994; Ito and Hotta, 1992; Lin et al., 2013; Sipe
576 and Siegrist, 2017). The majority of other NBs, however, enter a period of quiescence (Kunz et
577 al., 2012; Prokop and Technau, 1994; Ito and Hotta, 1992) and require dietary nutrients and
578 PI3-kinase activity to exit quiescence ~24 hrs after hatching (Lovick and Hartenstein, 2015; Sipe
579 and Siegrist, 2017). During subsequent larval development, each MB NBs generates an almost
580 identical repertoire of intrinsic Kenyon cells and continues to proliferate on into the pupal stages
581 (~85-90 hours after pupa formation) (Ito and Hotta, 1992; Ito et al., 1997). As a result, the adult
582 MB neuropil in each CB lobe is densely packed with around 2000-3000 Kenyon cells per lobe
583 (Technau and Heisenberg, 1982; Aso et al., 2009).

584 Thus the MB NBs (and AL NBs) are inherently different in their proliferative schedules
585 compared to the rest of the neuroblasts in the *Drosophila* larval brain. This may explain in part
586 their resilience to nucleolar stress; that is, continued neuroblast proliferation and already high
587 synthetic rates (e.g., ribosome production) may sustain the MB NBs upon nucleolar stress at
588 least temporarily, while the other NBs may not be able to rekindle high synthetic levels as they
589 exit quiescence (Bertoli et al., 2013).

590

591 **Phenotypes**

592 For the first time, we showed that the *Nopp140* gene in *Drosophila* is haplo-insufficient
593 where *J11^{DsRed}/TM3* displayed embryonic lethality (Fig. 4A). This was a surprise since a
594 previous segmental aneuploidy study indicated no haplo-insufficiency genes existed in
595 cytological region 78F4 of the left arm of chromosome 3 (Lindsley et al., 1972). Haplo-
596 insufficiency of the *Drosophila Nopp140* gene would be analogous to haplo-insufficiency of the
597 human *Tcof1* gene which encodes treacle, a vertebrate early RBF related to Nopp140 in
598 structure and function. Loss of treacle in *Tcof1*^{+/-} human embryos results in the Treacher
599 Collins syndrome, a ribosomopathy leading to apoptosis in select embryonic neural crest cells
600 ultimately leading to the craniofacial birth defects.

601 Earlier work in our lab showed that complete loss of Nopp140 in *Drosophila* induced
602 nucleolar stress with the redistribution of the C/D box methyl-transferase, fibrillarin, to the
603 nucleoplasm (He et al., 2015). Here, we showed that *Nopp140* transcripts and at least the
604 Nopp140-RGG isoform were reduced but not completely absent in early larvae homozygous for
605 the disrupted *Nopp140* allele, *J11^{non-DsRed}*, (Figs 2, 3). Interestingly, each wild type central brain
606 lobe showed four anterior cells that appeared to contain more Nopp140-RGG than other cells
607 within the same lobes (Fig. 3). The observation suggested that MB NBs contain more Nopp140
608 than do other NBs. We then showed that mCD8::GFP-labeled MB lineages in homozygous

609 *J11^{non-DsRed}* larvae retained nucleolar fibrillarin, whereas fibrillarin was noticeably redistributed to
610 the nucleoplasm in the majority of other NBs (Fig. 8). This latter observation indicated that
611 nucleoli in the MB lineages preferentially retained more RBFs and perhaps maintained
612 functional production of ribosomes longer, although to what extent requires future molecular
613 analyses.

614

615 **Differential Expressions**

616 Most cells within the central brain lobes of homozygous *J11^{non-DsRed}* larvae 1-2 day ALH
617 showed reduced anti-Nopp140-RGG labeling compared to brain cells in similarly aged wild type
618 larvae. Interestingly, wild type larvae clearly showed four cells, identified as MB NBs, per central
619 brain lobe with prominent anti-Nopp140-RGG labeling (Fig. 3). The observation suggests that
620 wild type MB NBs contain more zygotically expressed Nopp140 than do other NBs. Recent
621 findings supporting this notion show that various RBFs such as treacle, fibrillarin, Nop56, mbm,
622 and NS3 are overexpressed in stem cell and progenitor cell populations (Brombin et al., 2015;
623 Watanabe-Susaki et al., 2014; Wang et al., 2013; Johnson et al., 2018; Hovhanyan et al., 2014;
624 Hartl et al., 2013; Dixon et al., 2006), and that the quantity and spatiotemporal expression of
625 RBFs can vary in different stem cell or progenitor cell populations (Weiner et al., 2012; Bouffard
626 et al., 2018). A selective expression of not only Nopp140, but other RBFs such as fibrillarin,
627 Nop56, Nop60b (Fig. 9A) in MB NBs during the embryo-to-larva transition period may explain
628 the resilience of MB lineages to nucleolar stress later during larval development.

629 Related to differential expression of RBFs in stem cells and progenitor cells is the
630 perplexing problem of why some larvae homozygous for the disrupted *Nopp140* gene survive up
631 to day 24 ALH (Fig. 4B). While we have yet to pursue this question rigorously, we suspect these
632 *Nopp140*^{-/-} individuals may inherit more maternal *Nopp140* mRNA and/or protein, and this
633 may be a function of the nutrition and health of the mothers. Earlier work in our lab (McCain et
634 al., 2006) followed maternally expression of GFP-Nopp140 into embryogenesis, and we noted
635 then that the protein has a long lifespan, on the order of several days. Individual *Nopp140*^{-/-}
636 embryos that inherited extra maternal *Nopp140* transcripts or protein would likely produce more
637 ribosomes and survive longer.

638

639 **The Possibility of Heterogeneous Ribosomes**

640 Ribosomes are not all the same even within a single cell (Xue and Barna, 2012; Guo
641 2018). Werner et al. (2015) showed that the translation program of human embryonic stem
642 cells (hESCs) differentiating into neural crest cells changed after the depletion of KBTBD8, a

643 substrate adapter for the vertebrate-specific ubiquitin ligase, CUL3. CUL3 mono-ubiquitylates
644 human Nopp140 (NOLC1) and treacle, and forms a Nopp140-treacle platform that connects
645 RNA Pol I machinery with ribosome modification factors. Based on these results, the authors
646 hypothesized that the change in translational profile was the result of differential alteration of
647 ribosomes. Modifications such as rRNA pseudouridylation and methylation, or phosphorylation
648 and ubiquitylation of ribosomal proteins or ribosome-associated factors may ultimately
649 contribute to translational control of gene expression (Sloan et al., 2017). Thus, the abundance
650 of Nopp140 in different *Drosophila* neuroblasts could potentially lead to differential modifications
651 of the ribosome pool, and thus changes in the translational profile in different neuroblasts.

652 Finally, transcriptome profiles (Fig. 9 and Supplemental Fig. 5) of the different
653 *Drosophila* larval brain neuroblasts indicated that RBFs fibrillarin, Nop140, Nop60, and Nop56
654 are expressed at higher levels in the MB NBs. Of the ribosomal proteins, Rpl41 had the highest
655 expression levels in all brain cells, but was again highest in the MB NBs (indicated by an
656 asterisk in Supplemental Fig. S5). Are there heterogeneous pools of ribosomes within a
657 *Drosophila* larval brain? If so, it might explain why the MB NBs are more resilient to nucleolar
658 stress. The *Drosophila* nervous system should serve well to explore differential threshold
659 requirements for ribosome production.

660

661 **Competing Interests**

662 The authors declare no competing or financial interests.

663

664 **Funding**

665 This study was funded by the National Science Foundation, grant numbers MCB0919709 and
666 MCB1712975.

667

668

669

670

671

672

673

674

675

676

677 **References**

678

679 **Aso, Y., Grübel, K., Busch, S., Friedrich, A. B., Siwanowicz I. and Tanimoto, H.** (2009). The
680 mushroom body of adult *Drosophila* characterized by GAL4 drivers. *J. Neurogenet.* **23**, 156-172.

681

682 **Bachellerie, J. P., Cavallé, J. and Hüttenhofer, A.** (2002). The expanding snoRNA world.
683 *Biochimie.* **84**, 775-790.

684

685 **Bae, S., Park, J. and Kim, J-S.** (2014). Cas-OFFinder: a fast and versatile algorithm that
686 searches for potential off-target sites of Cas9 RNA-guided endonucleases. *Bioinformatics.* **30**,
687 1473–1475.

688

689 **Baßler, J. and Hurt, E.** (2019). Eukaryotic ribosome assembly. *Annu. Rev. Biochem.* **88**, 281-
690 306.

691

692 **Bertoli, C., Skotheim, J. M. and de Bruin, R. A. M.** (2013). Control of cell cycle transcription
693 during G1 and S phases. *Nat. Rev. Mol. Cell Biol.* **14**, 518-528.

694

695 **Birkholz, O., Rickert, C., Nowak, J., Coban, I. C. and Technau, G. M.** (2015). Bridging the
696 gap between postembryonic cell lineages and identified embryonic neuroblasts in the ventral
697 nerve cord of *Drosophila melanogaster*. *Biol. Open.* **4**, 420-434.

698

699 **Bouffard, S., Dambroise, E., Brombin, A., Lempereur, S., Hatin, I., Simion, M., Corre, R.,
700 Bourrat, F., Joly, J. S. and Jamen, F.** (2018). Fibrillarin is essential for S-phase progression
701 and neuronal differentiation in zebrafish dorsal midbrain and retina. *Dev. Biol.* **437**, 1-16.

702

703 **Brombin, A., Joly, J. S. and Jamen, F.** (2015). New tricks for an old dog: ribosome biogenesis
704 contributes to stem cell homeostasis. *Curr. Opin. Genet. Dev.* **34**, 61-70.

705

706 **Cui, Z. and DiMario, P. J.** (2007). RNAi knockdown of Nopp140 induces *Minute*-like
707 phenotypes in *Drosophila*. *Mol. Biol. Cell.* **18**, 2179-2191.

708

709 **Dauwerse, J. G., Dixon, J., Seland, S., Ruivenkamp, C. A., van Haeringer, A., Hoefsloot, L.
710 H., Peters, D. J., Boers, A. C., Daumwer-Haas, C., Maiwald, R., et al.** (2011). Mutations in

711 genes encoding subunits of RNA polymerases I and III cause Treacher Collins syndrome. *Nat.*
712 *Genet.* **43**, 20-22.

713

714 **de Cuevas, M. and Spradling, A. C.** (1998). Morphogenesis of the *Drosophila* fusome and its
715 implications for oocyte specification. *Development.* **125**, 2781-2789.

716

717 **Dixon, J., Jones, N. C., Sandell, L. L., Jayasinghe, S. M., Crane, J., Rey, J. P., Dixon, M. P.**
718 **and Trainor, P. A.** (2006). Tcof1/Treacle is required for neural crest cell formation and
719 proliferation deficiencies that cause craniofacial abnormalities. *Proc. Natl. Acad. Sci. USA.* **103**,
720 13403-13408.

721

722 **Doudna, J. A. and Charpentier, E.** (2014). The new frontier of genome engineering with
723 CRISPR-Cas9. *Science.* **346**, 1258096-1258096.

724

725 **Egger, B., Chell, J. M. and Brand, A. H.** (2008). Insights into neural stem cell biology from
726 flies. *Philos. Trans. R. Soc. B. Biol. Sci.* **363**, 39-56.

727

728 **Garneau, N. L., Wilusz, J. and Wilusz, C. J.** (2007). The highways and byways of mRNA
729 decay. *Nat. Rev. Mol. Cell Biol.* **8**, 113-126.

730

731 **Golomb, L., Volarevic, S. and Oren, M.** (2014). p53 and ribosome biogenesis stress: The
732 essentials. *FEBS Lett.* **588**, 2571-2579.

733

734 **Gonzales, B., Henning, D., So, R. B., Dixon, J., Dixon, M. J. and Valdez, B. C.** (2005). The
735 Treacher Collins syndrome (TCOF1) gene product is involved in pre-rRNA methylation. *Hum*
736 *Mol. Genet.* **14**, 2035-2043.

737

738 **Gratz, S. J., Cummings, A. M., Nguyen, J. N., Hamm, D. C., Donohue, L. K., Harrison, M.**
739 **M., Wildonger, J. and O'Connor-Giles, K.** (2013). Genome engineering of *Drosophila* with the
740 CRISPR RNA-guided Cas9 nuclease. *Genetics* **194**, 1029-1035.

741

742 **Gratz, S. J., Ukken, F. P., Rubinstein, C. D., Thiede, G., Donohue, L. K., Cummings, A. M.**
743 **and O'Connor-Giles, K. M.** (2014). Highly specific and efficient CRISPR/Cas9-catalyzed
744 homology-directed repair in *Drosophila*. *Genetics.* **196**, 961-971.

745
746 **Guo, H.** (2018). Specialized ribosomes and the control of translation. *Biochem. Soc. Trans.* **46**,
747 855-869.
748
749 **Hartenstein, V. and Wodarz, A.** (2013). Initial neurogenesis in *Drosophila*. *Wiley Interdiscip.*
750 *Rev. Dev. Biol.* **2**, 823-823.
751
752 **Hartl, T. A., Ni, J., Cao, J., Suyama, K. L., Patchett, S., Bussiere, C., Gui, D. Y., Tang, S.,**
753 **Kaplan, D. D., Johnson, A. W. and Scott, M. P.** (2013). Regulation of ribosome biogenesis by
754 nucleostemin 3 promotes local and systemic growth in *Drosophila*. *Genetics.* **194**, 101-115.
755
756 **Hayano, T., Yanagida, M., Yamauchi, Y., Shinkawa, T., Isobe, T. and Takahashi, N.** (2003).
757 Proteomic analysis of human Nop56p-associated pre-ribosomal ribonucleoprotein complexes. *J.*
758 *Biol. Chem.* **278**, 34309-34319.
759
760 **He, F. and DiMario, P. J.** (2011). *Drosophila* delta-1-pyrroline-5-carboxylate dehydrogenase
761 (P5CDh) is required for proline breakdown and mitochondrial integrity - Establishing a fly model
762 for human type II hyperprolinemia. *Mitochondrion.* **11**, 397-404.
763
764 **He, F., James, A., Raje, H., Ghaffari, H. and DiMario, P.** (2015). Deletion of *Drosophila*
765 Nopp140 induces subcellular ribosomopathies. *Chromosoma.* **124**, 191-208.
766
767 **Homem, C. C. and Knoblich, J. A.** (2012). *Drosophila* neuroblasts: a model for stem cell
768 biology. *Development.* **139**, 4297-4310.
769
770 **Hovhanyan, A., Herter, E. K., Pfannstiel, J., Gallant, P. and Raabe, T.** (2014). *Drosophila*
771 mbm is a nucleolar myc and casein kinase 2 target required for ribosome biogenesis and cell
772 growth of central brain neuroblasts. *Mol. Cell. Biol.* **34**, 1878-1891.
773
774 **Ito, K., Awano, W., Suzuki, K., Hiromi, Y. and Yamamoto, D.** (1997). The *Drosophila*
775 mushroom body is a quadruple structure of clonal units each of which contains a virtually
776 identical set of neurones and glial cells. *Development.* **124**, 761-771.
777

778 **Ito, K. and Hotta, Y.** (1992). Proliferation pattern of postembryonic neuroblasts in the brain of
779 *Drosophila melanogaster*. *Dev. Biol.* **149**, 134-148.
780

781 **James, A., Cindass, Jr. R., Mayer, D., Terhoeve, S., Mumphrey, C. and DiMario, P.** (2013).
782 Nucleolar stress in *Drosophila melanogaster*. *Nucleus.* **4**, 123-133.
783

784 **James, A., Wang, Y., Raje, H., Rosby, R. and DiMario, P.** (2014). Nucleolar stress with and
785 without p53. *Nucleus.* **5**, 402-426.
786

787 **Jinek, M., Chylinski, K., Fonfara, I., Hauer, M., Doudna, J. A. and Charpentier, E.** (2012). A
788 programmable dual-RNA-guided DNA endonuclease in adaptive bacterial immunity. *Science.*
789 **337**, 816-821.
790

791 **Johnson, P. W., Doe, C. Q. and Lai, S-L.** (2018). *Drosophila* nucleostemin 3 is required to
792 maintain larval neuroblast proliferation. *Dev. Biol.* **440**, 1-12.
793

794 **Jones, N. C., Lynn, M. L., Gaudenz, K., Sakai, D., Aoto, K., Rey, J. P., Glynn, E. F.,**
795 **Ellington, L., Du, C., Dixon, J., et al.** (2008). Prevention of the neurocristopathy Treacher
796 Collins syndrome through inhibition of p53 function. *Nat. Med.* **14**, 125-133.
797

798 **Kaplan, D. D., Zimmermann, G., Suyama, K., Meyer, T. and Scott, M. P.** (2008). A
799 nucleostemin family GTPase, NS3, acts in serotonergic neurons to regulate insulin signaling
800 and control body size. *Genes Dev.* **22**, 1877-1893.
801

802 **Knott, G. J. and Doudna, J. A.** (2018). CRISPR-Cas guides the future of genetic engineering.
803 *Science.* **361**, 866-869.
804

805 **Kressler, D., Hurt, E. and Baßler, J.** (2010). Driving ribosome assembly. *Biochim. Biophys.*
806 *Acta.* **1803**, 673-683.
807

808 **Kunz, T., Kraft, K. F., Technau, G. M. and Urbach, R.** (2012). Origin of *Drosophila* mushroom
809 body neuroblasts and generation of divergent embryonic lineages. *Development.* **139**, 2510-
810 2522.
811

- 812 **Lai, S.-L. and Doe, C. Q.** (2014). Transient nuclear Prospero induces neural progenitor
813 quiescence. *Elife*. **3**.
814
- 815 **Lambertsson, A.** (1998). The *Minute* genes in *Drosophila* and their molecular functions. *Adv.*
816 *Genet.* **38**, 69–134.
817
- 818 **Lin, S., Marin, E. C., Yang, C. P., Kao, C. F., Apenteng, B. A., Huang, Y., O'Connor, M. B.,**
819 **Truman, J. W. and Lee, T.** (2013). Extremes of lineage plasticity in the *Drosophila* brain. *Curr.*
820 *Biol.* **23**, 1908-1913.
821
- 822 **Lindsley, D. L., Sandler, L., Baker, B. S., Carpenter, A. T. C., Denell, R. E., Hall, J. C.,**
823 **Jacobs, P. A., Miklos, G. L., Davis, B. K., Gethmann, R. C. et al.** (1972). Segmental
824 aneuploidy and the genetic gross structure of the *Drosophila* genome. *Genetics.* **71**, 157-184.
825
- 826 **Long, E. O. and Dawid, I. B.** (1980). Alternative pathways in the processing of ribosomal RNA
827 precursor in *Drosophila melanogaster*. *J. Mol. Biol.* **138**, 873–878.
828
- 829 **Lovick, J. K. and Hartenstein, V.** (2015). Hydroxyurea-mediated neuroblast ablation
830 establishes birthdates of secondary lineages and addresses neuronal interactions in the
831 developing *Drosophila* brain. *Dev. Biol.* **402**, 32-47.
- 832 **MacInnes, A. W.** (2016). The role of the ribosome in the regulation of longevity and lifespan
833 extension. *Wiley Interdiscip. Rev. RNA.* **7**, 198-212.
- 834 **Marygold, S. J., Roote, J., Reuter, G., Lambertsson, A., Ashburner, M., Millburn, G. H.,**
835 **Harrison, P. M., Yu, Z., Kenmochi, N., Kaufman, T. C., et al.** (2007). The ribosomal protein
836 genes and *Minute* loci of *Drosophila melanogaster*. *Genome Biol.* **8**, R216.
837
- 838 **McCain, J., Danzy, L., Hamdi, A., Dellafosse, O. and DiMario, P.** (2006). Tracking nucleolar
839 dynamics with GFP-Nopp140 during *Drosophila* oogenesis and embryogenesis. *Cell Tissue*
840 *Res.* **323**, 105-115.
841
- 842 **McCann, K. L. and Baserga, S. J.** (2013). Mysterious ribosomopathies. *Science.* **341**, 849-850.
843

844 **Meier, U. T.** (1996). Comparison of the rat nucleolar protein Nopp140 with its yeast homolog
845 SRP40. *J. Biol. Chem.* **271**, 19376-19384.
846

847 **Narla, A. and Ebert, B. L.** (2010). Ribosomopathies: Human disorders of ribosome dysfunction.
848 *Blood.* **115**, 3196-3205.
849

850 **Noack Watt, K. E., Achilleos, A., Neben, C. L., Merrill, A. E. and Trainor, P. A.** (2016). The
851 roles of RNA polymerase I and III subunits Polr1c and Polr1d in craniofacial development and in
852 zebrafish models of Treacher Collins Syndrome. *PLoS Genet.* **12**, e1006187.
853

854 **Port, F., Chen, H. M., Lee, T. and Bullock, S. L.** (2014). Optimized CRISPR/Cas tools for
855 efficient germline and somatic engineering in *Drosophila*. *Proc. Natl. Acad. Sci. USA* **111**,
856 E2967-E2976.
857

858 **Prokop, A. and Technau, G. M.** (1994). Normal function of the mushroom body defect gene of
859 *Drosophila* is required for the regulation of the number and proliferation of neuroblasts. *Dev.*
860 *Biol.* **161**, 321-337.
861

862 **Reimer, G., Pollard, K. M., Penning, C. A., Ochs, R. L., Lischwe, M. A., Busch, H. and Tan,**
863 **E. M.** (1987). Monoclonal autoantibody from a (New Zealand black x New Zealand white) F₁
864 mouse and some scleroderma sera target an M_r 34,000 nucleolar protein of the U3 RNP
865 particle. *Arthritis Rheum.* **30**, 793-800.
866

867 **Ren, X., Sun, J., Housden, B. E., Hu, Y., Roesel, C., Lin, S., Liu, L. P., Yang, Z., Mao, D.,**
868 **Sun, L., et al.** (2013). Optimized gene editing technology for *Drosophila melanogaster* using
869 germ line-specific Cas9. *Proc. Natl. Acad. Sci. USA* **110**, 19012-19017.
870

871 **Renault, A. D.** (2012). *vasa* is expressed in somatic cells of the embryonic gonad in a sex-
872 specific manner in *Drosophila melanogaster*. *Biol. Open.* **1**, 1043-1048.
873

874 **Rosby, R., Cui, Z., Rogers, E., deLivion, M. A., Robinson, V. L. and DiMario, P. J.** (2009).
875 Knockdown of the *Drosophila* GTPase nucleostemin 1 impairs large ribosomal subunit
876 biogenesis, cell growth, and midgut precursor cell maintenance. *Mol. Biol. Cell.* **20**, 4424-4434.
877

- 878 **Sakai, D. and Trainor, P. A.** (2009). Treacher Collins syndrome: unmasking the role of
879 Tcof1/treacle. *Int. J. Biochem. Cell Biol.* **41**, 1229-1232.
- 880
- 881 **Sipe, C. W. and Siegrist, S. E.** (2017). Eyeless uncouples mushroom body neuroblast
882 proliferation from dietary amino acids in *Drosophila*. *Elife*. **6**, e26343.
- 883
- 884 **Sloan, K. E., Warda, A. S., Sharma, S., Entian, K-D., Lafontaine, D. L. J. and Bohnsack, M.**
885 **T.** (2017). Tuning the ribosome: The influence of rRNA modification on eukaryotic ribosome
886 biogenesis and function. *RNA Biol.* **14**, 1138-1152.
- 887
- 888 **Technau, G. and Heisenberg, M.** (1982). Neural reorganization during metamorphosis of the
889 corpora pedunculata in *Drosophila melanogaster*. *Nature*. **295**, 405-407.
- 890
- 891 **Thum, A. S. and Gerber, B.** (2019). Connectomics and function of a memory network: the
892 mushroom body of larval *Drosophila*. *Curr. Opin. Neurobiol.* **54**, 146-154.
- 893
- 894 **Tsai, R. Y. L. and Pederson, T.** (2014). Connecting the nucleolus to the cell cycle and human
895 disease. *FASEB J.* **28**, 3290-3296.
- 896
- 897 **Tsai, R. Y. L.** (2011). New frontiers in nucleolar research: nucleostemin and related proteins. In
898 *The Nucleolus* (ed. M. O. J. Olson), pp. 301-320. New York: Springer.
- 899
- 900 **Urbach, R. and Technau, G. M.** (2003). Molecular markers for identified neuroblasts in the
901 developing brain of *Drosophila*. *Development*. **130**, 3621-3637.
- 902
- 903 **Waggener, J. M. and DiMario, P. J.** (2002). Two splice variants of Nopp140 in *Drosophila*
904 *melanogaster*. *Mol. Biol. Cell.* **13**, 362-381.
- 905
- 906 **Wang, C., Query, C. C. and Meier, U. T.** (2002). Immunopurified small nucleolar
907 ribonucleoprotein particles pseudouridylate rRNA independently of their association with
908 phosphorylated Nopp140. *Mol. Cell. Biol.* **22**, 8457-8466.
- 909
- 910 **Wang, H. D., Kazemi-Esfarjani, P. and Benzer, S.** (2004). Multiple-stress analysis for isolation
911 of *Drosophila* longevity genes. *Proc. Natl. Acad. Sci. USA.* **101**, 12610-12615.

912
913 **Wang, H., Chen, X., He, T., Zhou, Y. and Luo, H.** (2013). Evidence for tissue-specific
914 Jak/STAT target genes in *Drosophila* optic lobe development. *Genetics*. **195**, 1291-1306.
915
916 **Wang, Y. and DiMario, P.** (2017). Loss of *Drosophila* nucleostemin 2 (NS2) blocks nucleolar
917 release of the 60S subunit leading to ribosome stress. *Chromosoma*. **126**, 375-388.
918
919 **Warner, J. R.** (1999). The economics of ribosome biosynthesis in yeast. *Trends Biochem. Sci.*
920 **24**, 437-440.
921
922 **Watanabe-Susaki, K., Takada, H., Enomoto, K., Miwata, K., Ishimine, H., Intoh, A., Ohtaka,**
923 **M., Nakanishi, M., Sugino, H., Asashima, M., et al.** (2014). Biosynthesis of ribosomal RNA in
924 nucleoli regulates pluripotency and differentiation ability of pluripotent stem cells. *Stem Cells*.
925 **32**, 3099-3111.
926
927 **Weiner, A. M., Scampoli, N. L. and Calcaterra, N. B.** (2012). Fishing the molecular bases of
928 Treacher Collins syndrome. *PLoS One*. **7**, e29574.
929
930 **Werner, A., Iwasaki, S., McGourty, C. A., Medina-Ruiz, S. Teerikorpi, N., Fedrigo, I.,**
931 **Ingolia, N. T. and Rape, M.** (2015). Cell-fate determination by ubiquitin-dependent regulation of
932 translation. *Nature*. **525**, 523-527.
933
934 **Woolford, J. L. Jr. and Baserga, S. J.** (2013). Ribosome biogenesis in the yeast
935 *Saccharomyces cerevisiae*. *Genetics*. **195**, 643-681.
936
937 **Xue, S. and Barna, M.** (2012). Specialized ribosomes: a new frontier in gene regulation and
938 organismal biology. *Nat. Rev. Mol. Cell Biol.* **13**, 355-369.
939
940 **Yang, C. P., Fu, C. C., Sugino, K., Liu, Z., Ren, Q., Liu, L. Y., Yao, X., Lee, L. P. and Lee, T.**
941 (2016). Transcriptomes of lineage-specific *Drosophila* neuroblasts profiled by genetic targeting
942 and robotic sorting. *Development*. **143**, 411-421.
943
944 **Yang, K., Yang, J. and Yi, J.** (2018). Nucleolar Stress: hallmarks, sensing mechanism and
945 diseases. *Cell Stress*. **2**, 125-140.

946

947 **Yang, Y., Isaac, C., Wang, C., Dragon, F., Pogačić, V. and Meier, U. T.** (2000). Conserved
948 composition of mammalian Box H/ACA and Box C/D small nucleolar ribonucleoprotein particles
949 and their interaction with the common factor Nopp140. *Mol. Biol. Cell.* **11**, 567-577.

950

951 **Zhong, W. and Chia, W.** (2008). Neurogenesis and asymmetric cell division. *Curr. Opin.*
952 *Neurobiol.* **18**, 4-11.

953

954

955 **Figure Legends**

956

957 **Fig. 1. Anatomy of the *Drosophila* larval brain and overall hypothesis.** **A** Larval brains have
958 two central brain lobes and a ventral nerve cord (VNC). There are roughly five neuroblast (NB)
959 types within the larval brain: Type I (grey), Type II (red), Mushroom body (green), Antennal lobe
960 (neon), and Optic lobe (blue). These NBs are shown in their putative locations within the larval
961 brain. **B** Our hypothesis is that upon nucleolar stress due to loss of Nopp140, different
962 neuroblast lineages exhibit variable phenotypes ranging from a mild to severe loss of lineage
963 progeny cells, to complete loss of the lineage altogether.

964

965 **Fig. 2. CRISPR-mediated disruption of the *Nopp140* gene and RT-PCR analysis.** **A** Three
966 plasmids encoding guide RNAs, gRNA#52 and gRNA#99, or the DsRed protein were injected
967 into embryos from the *nanos-Cas9* fly line. The guide RNAs directed Cas9 cleavage at two
968 specific sites located 321 base pairs apart in the second exon of the *Nopp140* gene (blue bar;
969 1650 bp total). The *DsRed* gene (red arrow) with flanking plasmid sequences (light grey) and 3'
970 and 5' *Nopp140* homology arms inserted into the deletion by homology directed repair (HDR).
971 Seven heterozygous *Nopp140* disruption lines were identified by DsRed expression in adult
972 eyes. The *DsRed* gene was subsequently mutated (dark grey arrow) by CRISPR-mediated
973 mutagenesis. **B** Genomic PCRs using a *DsRed*-specific forward primer (grey) and a
974 downstream *Nopp140*-specific reverse primer (blue half arrow in panel A) verified the *DsRed*
975 insertion within the second exon of *Nopp140* gene in all seven *Nopp140* heterozygous
976 disruption lines (*J11*, *J47*, *J54*, *J60*, *K13*, *M6*, *M20*) with the expected 1836 bp product. The
977 *w¹¹¹⁸* fly line served as negative control. **C** RT-PCR analyses of *Nopp140* transcript levels in
978 control *w¹¹¹⁸* and homozygous *J11^{non-DsRed}* larvae day 1-2 ALH using the Exon2 reverse primer
979 (blue half arrow) for first strand cDNA synthesis. Subsequent PCRs used the same Exon2

980 reverse primer and a forward primer specific for the first intron of the *Nopp140* gene. A
981 representative gel is provided. No PCR products appeared in the minus-RT controls. Band
982 intensity ratios ($J11/w^{1118}$) were determined for three biological replicates with overall mean +/-
983 SEM of 0.61+/-0.022. Student's t-test: two-tailed with equal variance for three biological
984 replicates (1, 2, 3) with three PCR technical replicates each, p-values = 0.037*, 0.00081**,
985 0.0064*** respectively. No RT-PCR product was detected using the pDsRed reverse primer
986 (grey half arrow) in the $J11^{non-DsRed}$ disruption line. **D** RT-PCR analyses of *ETS*, *ITS2*, *Hsp26*,
987 *RpL32*, and *Actin5C* transcript levels were carried out in control w^{1118} larvae at day 1-2 ALH and
988 in homozygous $J11^{DsRed}$ larvae at two time points, day 1-2 and 5-7 ALH using gene-specific
989 reverse primers. Three biological replicates were performed. For each replicate, total RNA was
990 extracted from ~300 w^{1118} and 150-300 homozygous $J11$ larvae. PCR reactions were carried
991 out in triplicate for each first strand cDNA. Representative gels are shown.

992

993 **Fig. 3. Maternal Nopp140 protein is reduced in early $J11$ *Nopp140*^{-/-} larval brains.** Central
994 brain lobes and mid-gut tissues from w^{1118} control (a-j, e-n) and homozygous $J11^{non-DsRed}$ larvae
995 (c-l, g-p) at day 1-2 (a-h) and day 4-5 (i-p) ALH were immunostained with anti-Nopp140-RGG.
996 Arrow in **panel a** indicates four neuroblasts per wild type brain lobe with large nucleoli labeled
997 with anti-Nopp140-RGG. n=19 (w^{1118}); n=23 (homozygous $J11^{non-DsRed}$); 2 technical replicates.
998 Scale bars: 10 μ m in panels a-f, m-p; 25 μ m in panels g-l

999

1000 **Fig. 4. Embryonic and larval survival upon complete or partial loss of Nopp140.** **A** Survival
1001 assays were performed for homozygous $J11^{DsRed}$ or heterozygous $J11^{DsRed}/TM3-GFP$ embryos,
1002 and for w^{1118} control embryos. Freshly laid eggs were collected from well-yeasted juice plates (n
1003 = 2; total number of embryos per replicate for w^{1118} : 200 and 299, and for $J11^{DsRed}/TM3-GFP$
1004 stock: 230 and 111). The number of hatched larvae were logged for the next two days, and the
1005 percent viable embryos was determined. Data shows the number of larvae hatched divided by
1006 the total number of embryos collected X 100%. **B** Plot shows three replicates (number of larvae
1007 per replicate: 70, 42, 62) of survival assay for homozygous $J11^{DsRed}$ larvae. Newly hatched
1008 larvae were collected from a well-yeasted juice plates, and the number of living larvae were
1009 recorded in the following days until all larvae had perished. **C** Embryonic lethality and larval
1010 survivability upon Nopp140 depletion by RNAi expression using the *worniu::GAL4* driver
1011 (specific for all embryonic and larval neuroblasts) and *UAS::TComC4.2* (Nopp140-RNAi line;
1012 Cui and DiMario 2007). Compared to 86.7% of the w^{1118} embryos, only 46.8% of the collected
1013 embryos with Nopp140 depletion (*worniu-GAL4>C4.2*) hatched and developed into 3rd instar

1014 larvae, after which all larvae developed into adults (not shown). n = 3; total number of embryos
1015 collected per replicate for each genotype: 200, 265, and 330; Student's t-test: two-tailed with
1016 unequal variance, p-value = 0.0069

1017

1018 **Fig. 5. *Drosophila* larval brain development is impaired under nucleolar stress induced by**

1019 **the loss of Nopp140. A** Larval brain development in homozygous *KO121* (*Nopp140* gene
1020 deletion, He et al. 2015), homozygous *J11* (CRISPR-mediated *Nopp140* disruption), and wild-
1021 type (*w¹¹¹⁸*) starting at day 1 after larval hatching (ALH) until day 7 and day 13 ALH.

1022 Homozygous *KO121* and *J11* larval brains at day 13 ALH are shown, but wild-type individuals
1023 have developed into adults by day 13 ALH, hence an adult fly brain is shown. **B** RNAi-depletion

1024 of Nopp140 using pan-neuronal GAL4 driver, *Neurotactin (Nrt)::GAL4*, and the *UAS::TComC4.2*

1025 (*Nopp140* RNAi line) resulted in impaired larval brain development similar to that seen in

1026 *Nopp140* homozygous deletion background. Representative larval brains from three

1027 independent crosses at day 4-5 ALH comparing *Nopp140*-depleted brains with control sibling

1028 brains (not expressing RNAi) are shown. Scale bar: 100 μ m **C** Conventional fluorescence

1029 images of the neuropil immunostained with antibody against Discs large (Dlg; green) in second

1030 instar *w¹¹¹⁸* control larvae and homozygous *J11^{DsRed}* larvae at day 2-3 ALH. White arrows show

1031 unstained peripheral cell body layers which are reduced in homozygous *J11^{non-DsRed}* larvae. n=15

1032 (wild-type); n=18 (homozygous *J11^{non-DsRed}*); >3 technical replicates. Scale bar: 50 μ m

1033

1034 **Fig. 6. Neuroblast proliferation is reduced upon nucleolar stress.** Confocal images of

1035 homozygous *J11^{DsRed}* and control *w¹¹¹⁸* larval brains at day 1 (a-f), 2-3 (g-l), and 6 (m-r) ALH are

1036 shown after EdU-labeling (Click-iT Alexa Fluor 488) followed by anti-Deadpan (anti-Dpn)

1037 immunostaining. Dpn-stained cells (magenta) are neuroblasts. After a 2 hr pulse, EdU-labeled

1038 S-phase cells (green) were committed to cell division. Arrows indicate four likely Mushroom

1039 Body NBs that were EdU- and Dpn-positive and clustered near the anterior of the central brain

1040 (a, b, d, e, g, h). Arrowheads indicate a few EdU-positive cells, likely arising from AL MBs, at the

1041 lateral side of the central brain (b, e, h). n=10, 15, and 10 for day 1, 2-3, and 6 respectively for

1042 both wild-type and homozygous *J11^{DsRed}* sample; 3 technical replicates. Scale bar: 50 μ m

1043

1044 **Fig. 7. Mushroom Body NBs are resilient to nucleolar stress.** Larval brains from control *w¹¹¹⁸*

1045 and homozygous *J11^{non-DsRed}* larvae (see the cross scheme in Supplementary Fig S4) at day 3

1046 ALH were used for 30 min EdU pulse labeling (Click-iT Alexa Fluor 594). Merged confocal

1047 images show EdU-labeled cells (magenta) nestled within the GFP-labeled MB lineage (green)

1048 near the anterior of the central brains. n=12 (control); n=20 (homozygous *J11^{non-DsRed}*); 3
1049 technical replicates. Scale bars: 50 μ m in panels a-d, 25 μ m in panels e-h

1050

1051 **Fig. 8. Mushroom Body lineage cells retain nucleolar fibrillarin under nucleolar stress.**

1052 Larval brains from control *w¹¹¹⁸* (whole brain in a-c; a central brain lobe in g-j) and homozygous
1053 *J11^{non-DsRed}* larvae (whole brain in d-f; a central brain lobe in k-n) at day 3 ALH were
1054 immunostained with anti-fibrillarin (magenta). Merged images in panels j and n were obtained
1055 from confocal images g and h, and k and l respectively. Arrows in the homozygous *J11^{non-DsRed}*
1056 larval brains (k, n) indicate nucleolar fibrillarin retained in the MB lineage cells marked by cell
1057 surface protein, mCD8::GFP (green), whereas fibrillarin is redistributed into the nucleoplasm in
1058 surrounding cells. n=10 (wild-type); n=10 (homozygous *J11^{non-DsRed}*); 2 technical replicates.
1059 Scale bars: 50 μ m in panels a-j, 25 μ m in panels k-n

1060

1061 **Fig. 9. Transcriptome analyses of ribosome biogenesis factors in lineage-specific**

1062 ***Drosophila* neuroblasts and neurons.** Expression levels of *Nopp140*, *fibrillarin*, *Nop56*, and
1063 *Nop60B* transcripts (A); *NS1*, *NS2*, *NS3*, and *NS4* transcripts (B); *Deadpan*, *Prospero*, and *Elav*
1064 (C) in the *Drosophila* larval NBs and neurons. All NB (n=3), Mushroom Body (MB) NB (n=3),
1065 Antennal Lobe (AL) NB (n=3), Type II NB (n=3), neurons (n=2). Transcriptome data obtained
1066 from Yang et al. (2016).

1067

1068

1069

1070

1071

1072

1073

1074

1075

1076

1077

1078

1079

1080

1081

1082 **Table 1. List of primers and their sequences.**

1083

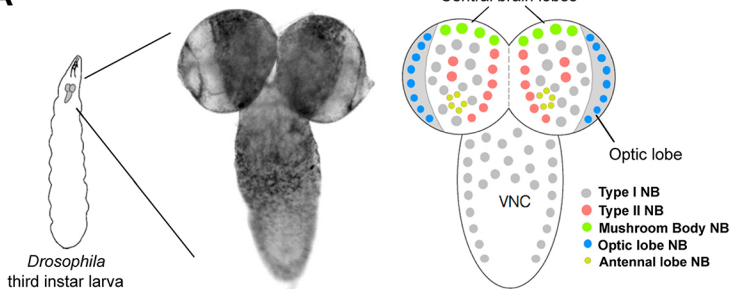
Primer	Sequence
gRNA-target#52sense	5' GTCGGGGCTTTGCCGGTTCTTCCT 3'
gRNA-target#52antisense	5' AAACAGGAAGAACCGGCAAAGCCC 3'
gRNA-target#99sense	5' GTCGCAAGTTGGCTCCTGCTAAGA 3'
gRNA-target#99antisense	5' AAACTCTTAGCAGGAGCCAACTTG 3'
DsRed target-gRNA#2 sense	5' GTCGGCTGAAGGTGACCAAGGG 3'
DsRed target-gRNA#2 antisense	5' AAACCCCTTGGTCACCTTCAGC 3'
DsRed target-gRNA#3 sense	5' GTCGGCTCCCACTTGAAGCCCT 3'
DsRed target-gRNA#3 antisense	5' AAACAGGGCTTCAAGTGGGAGC 3'
DsRed-Forward	5' GTGTAGTTCTCGTTGTGGGAGGTGAT 3'
DsRed-Reverse	5' GTGTAGTTCTCGTTGTGGGAGGTGAT 3'
Nopp140-Exon2-1556	5' TTCTCATTGCCATTGGTAGC 3'
First Intron-Forward	5' ATCTGCGTCCTCCTGATC 3'
Exon2	5' CTCGGAAGTCTATCCTCGCTG 3'
pDsRed	5' GTATGCTATACGAAGTTATAGAAGAGC 3'
5'HomologyArm-EcoRI-F	5' GGTGGAATTCGTCTTCGCTTGAAGACTTGGCCT 3'
5'HomologyArm-NotI-R	5' GTATGCGGCCGCAGAAGGGGGCTTCCTCTAGT 3'
3'HomologyArm-BglII-F	5' GTAAAGATCTCCTCGGAAGTCTATCCTCGCTGC 3'
3'HomologyArm-XhoI-R	5' GAGTCTCGAGGCCAGTGTCCGAAAAGCAG 3'
ETS-Forward	5' TGCCGACCTCGCATTGTTCGAAATW 3'
ETS-Reverse	5' ACCGAGCGCACATGATAATTCTTCCW3'
ITS2-Forward	5' TGGAGTACTATGGTTGAGGGTTG 3'
ITS2-Reverse	5' CGAACCAACGAAGAATAATAACATAACC 3'
Hsp26-Forward	5' CCCCATCTACGAGCTTGGACTG 3'
Hsp26-Reverse	5' TGTAGCCATCGGGAACCTTGTAGC 3'
RpL32-Forward	5' GTTGTGCACCAGGAACCTTCTTGAATCCG 3'
RpL32-Reverse	5' CTTCCAGCTTCAAGATGACCATCCGC 3C
Actin5C-Forward	5' CTCACCTATAGAAGACGAAGAAGTTGCTGCTCT 3'
Actin5C-Reverse	5' CTAAGTGTGAATCCTCGTAGGACTTCTCCAACG 3'

1084

1085

Figure 1

A



B

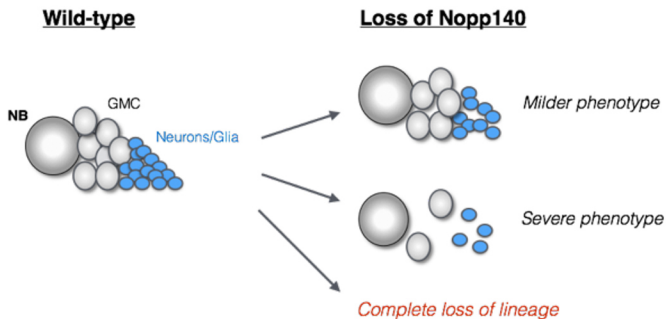
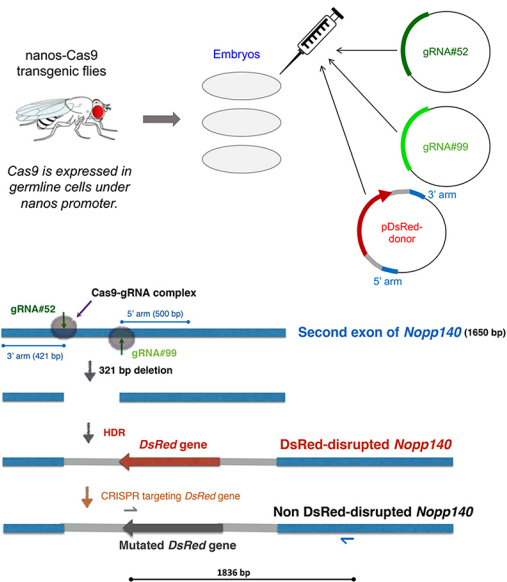
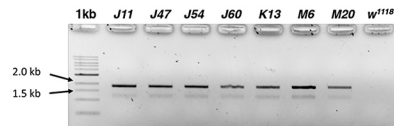


Figure 2

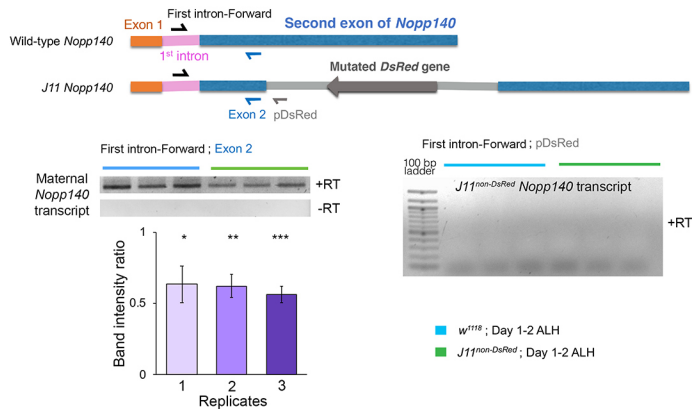
A



B



C



D



Figure 3

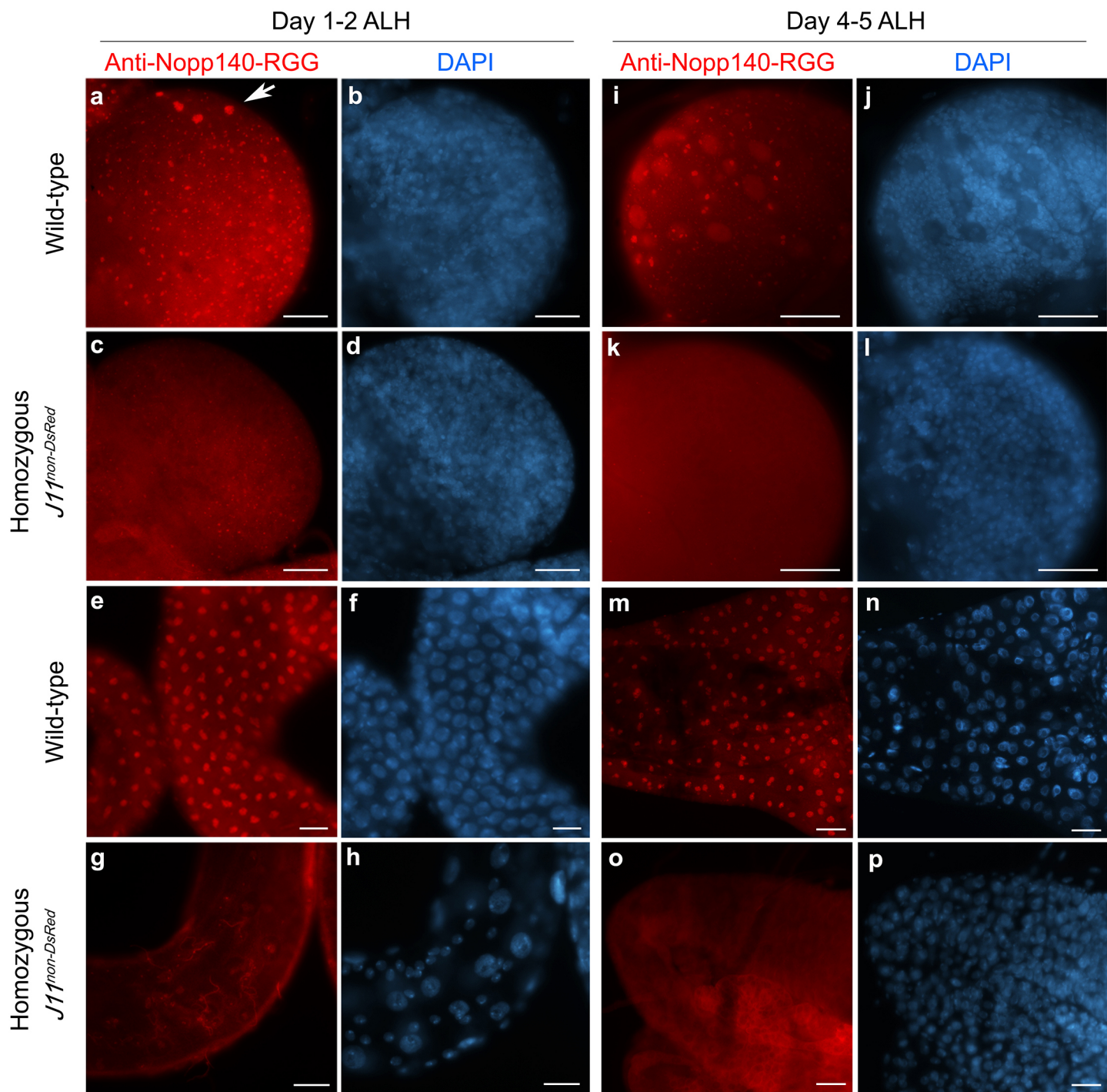
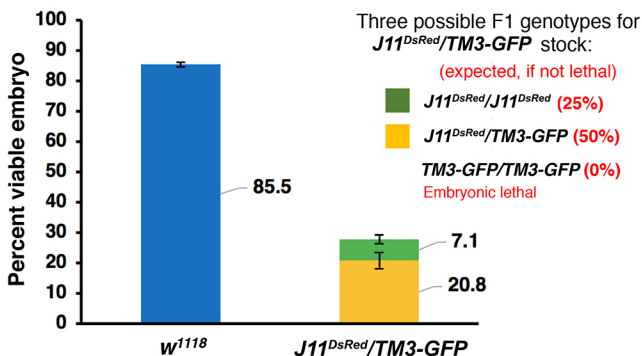
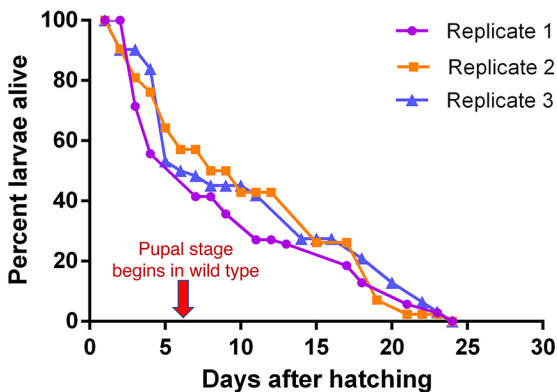


Figure 4

A



B



C

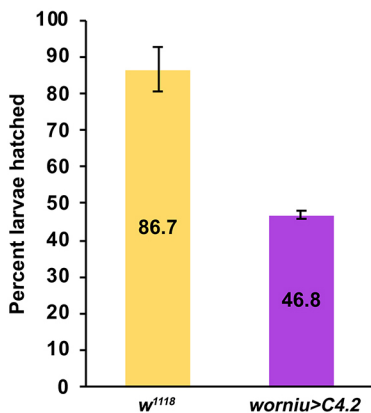
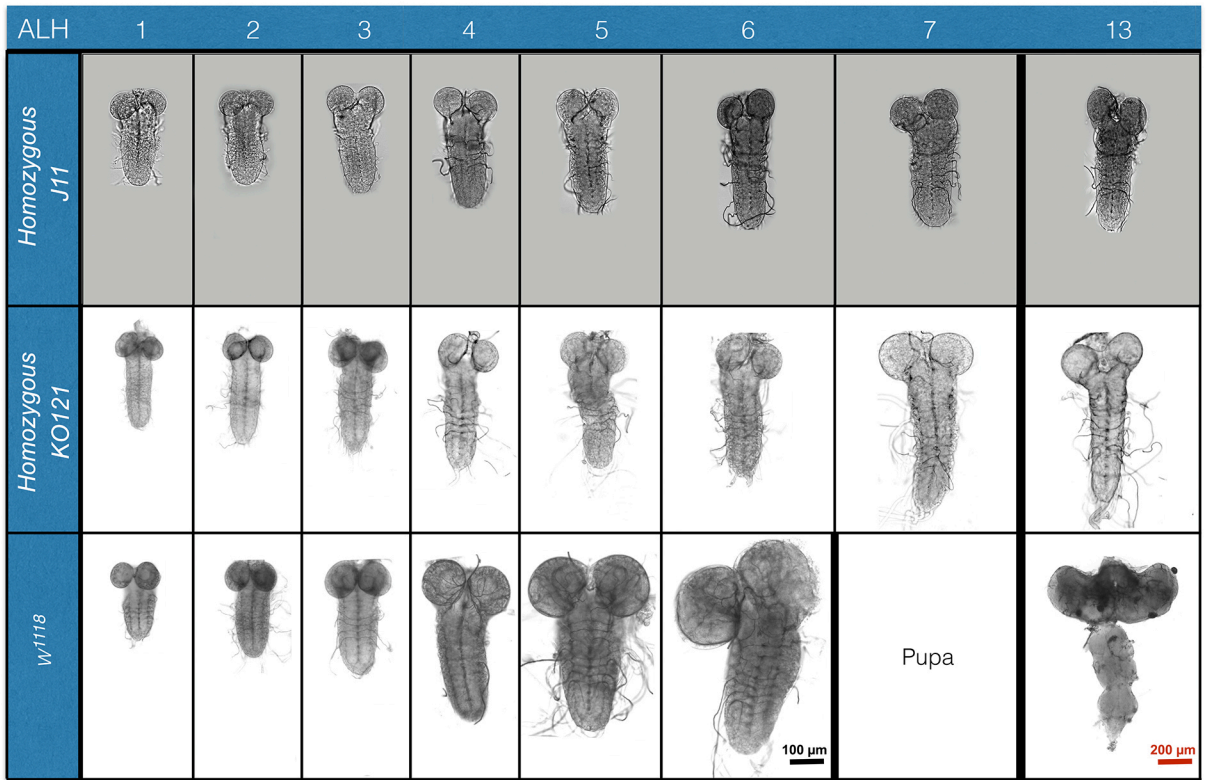
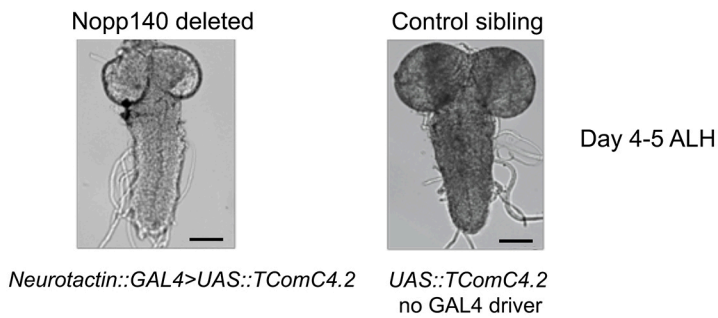


Figure 5

A



B



C

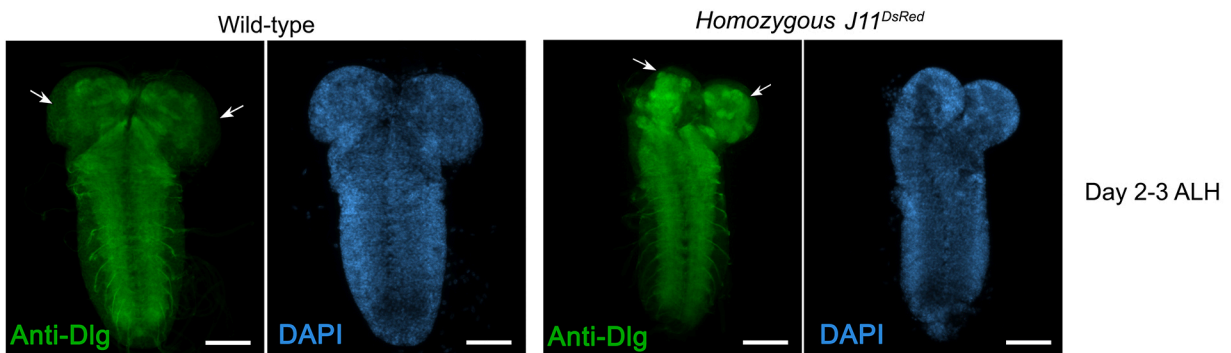


Figure 6

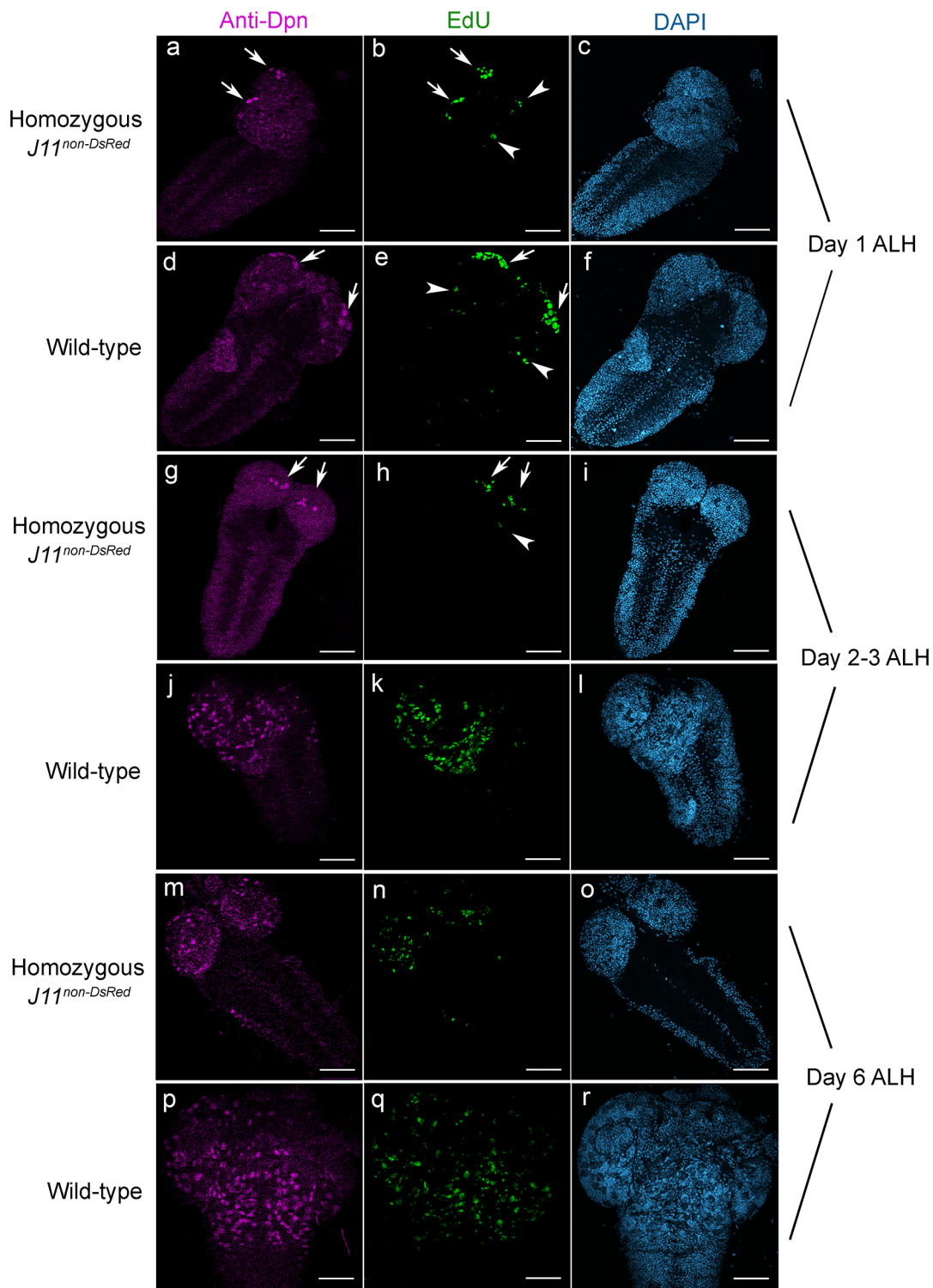


Figure 7

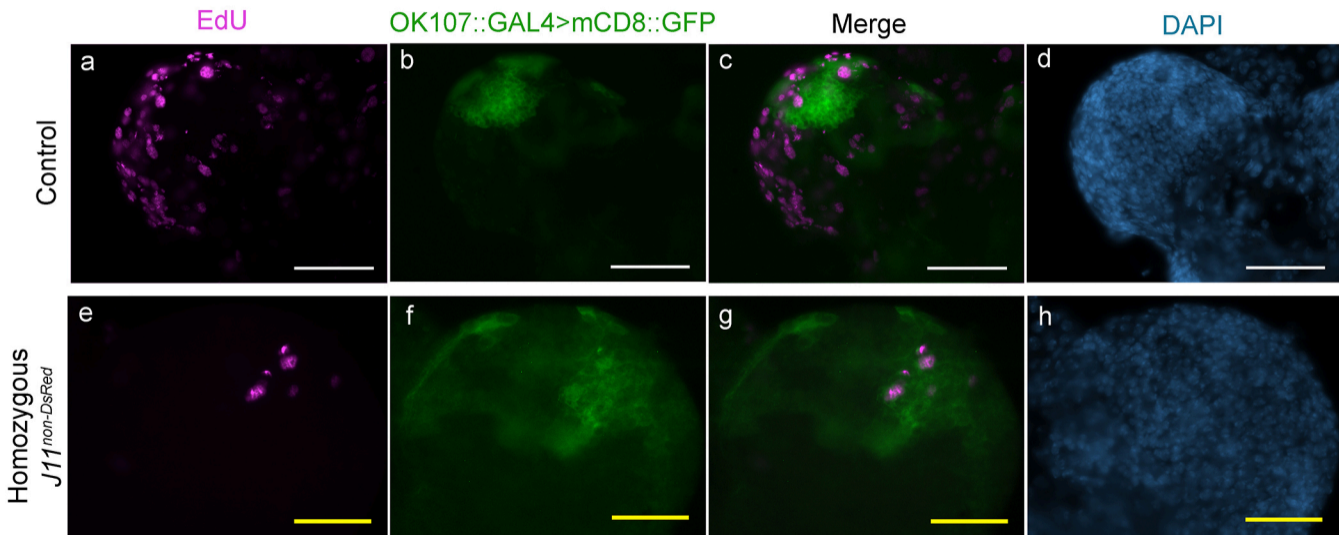
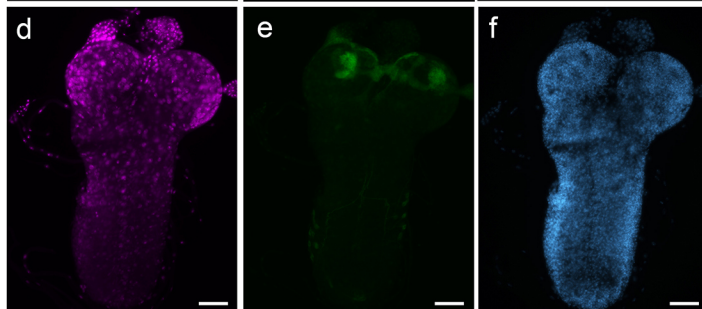
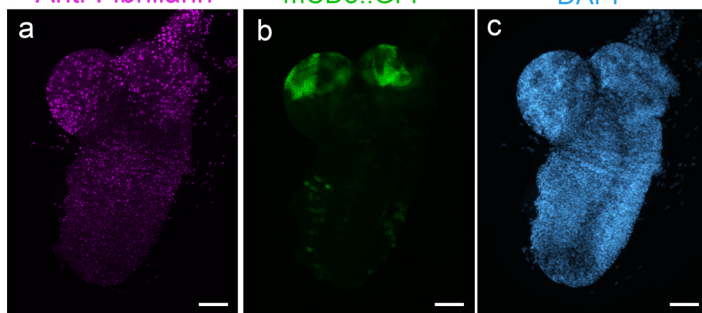


Figure 8

Anti-Fibrillarlin

OK107::GAL4>
mCD8::GFP

DAPI



Merge

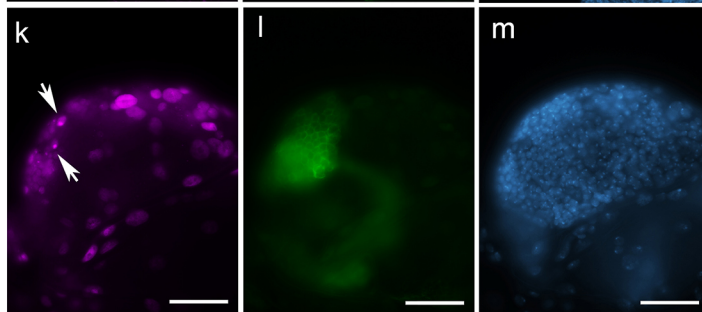
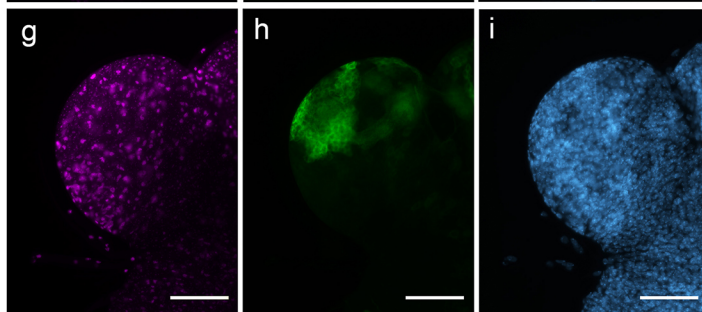


Figure 9

